Chapter 2

Building Models

This chapter describes the steel moment-resisting frame (MRF) building designs and the nonlinear finite element models of the buildings used in this thesis. The models represent buildings of shorter and taller height, and they represent stiffer, higher-strength and more flexible, lower-strength designs. I do not discuss the responses of these four buildings as individual designs. Rather, I consider the responses in comparison: how do shorter buildings behave compared to taller buildings; how do stiffer, higher-strength designs compare to more flexible, lower-strength designs; and how do buildings with fracture-prone welds compare to those with sound welds?

The second half of this chapter characterizes the building models and how they are used in this thesis. I report the first and second elastic modal periods and show pushover curves of the models. I also discuss the deformed shape of steel MRF buildings under an idealized pulse excitation because this type of ground motion induces an important collapse mechanism in these buildings. There are several decisions about how to model the seismic response of steel MRFs that may affect the conclusions. I identify some of these initial decisions, or modeling assumptions, and study the sensitivity of the building responses to these assumptions.

2.1 Building Designs

Hall (1997) designed four steel MRF buildings. Each building has either six or twenty above-ground stories, and the design of the lateral force-resisting system conforms

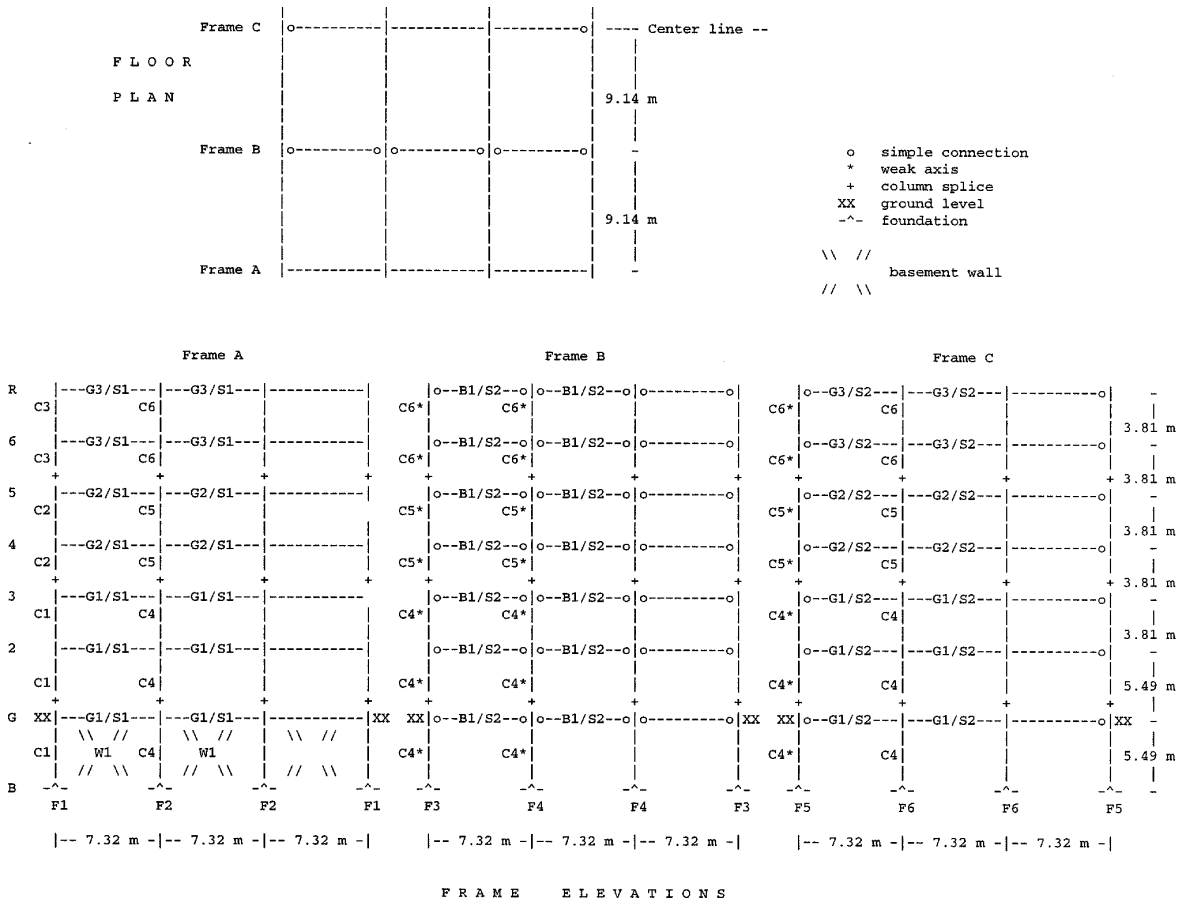

Figure 2.1: This six-story building (J6), designed to the 1992 JBC seismic provisions, is stiffer and stronger than the equivalent building designed to the 1994 UBC (U6). Reproduced from Hall (1997).

to either the 1992 Japanese Building Code (JBC) or 1994 Uniform Building Code (UBC) seismic provisions. This section describes the properties of the building designs as distinct from the finite element models of the buildings. All buildings have a rectangular floor plan and are regular in plan and elevation (Figures 2.1–2.4). Appendix A lists the beam and column schedules. The buildings consist of several frames. The perimeter frames have moment-resisting joints. The interior frames mostly have simply-supported joints.

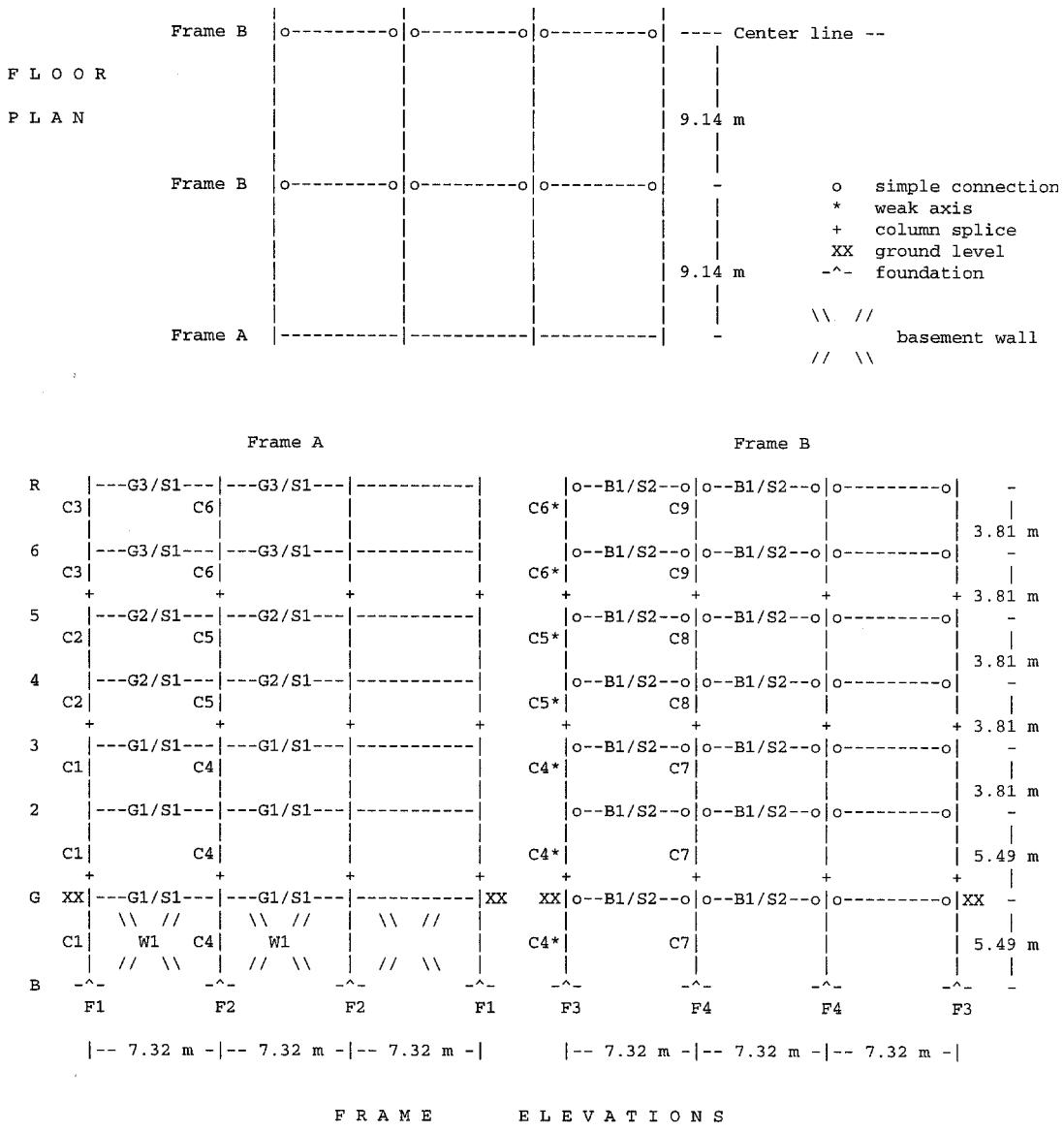

Figure 2.2: This six-story building (U6), designed to the 1994 UBC seismic provisions, is more flexible and has a lower-strength than the equivalent building designed to the 1992 JBC. Reproduced from Hall (1997).

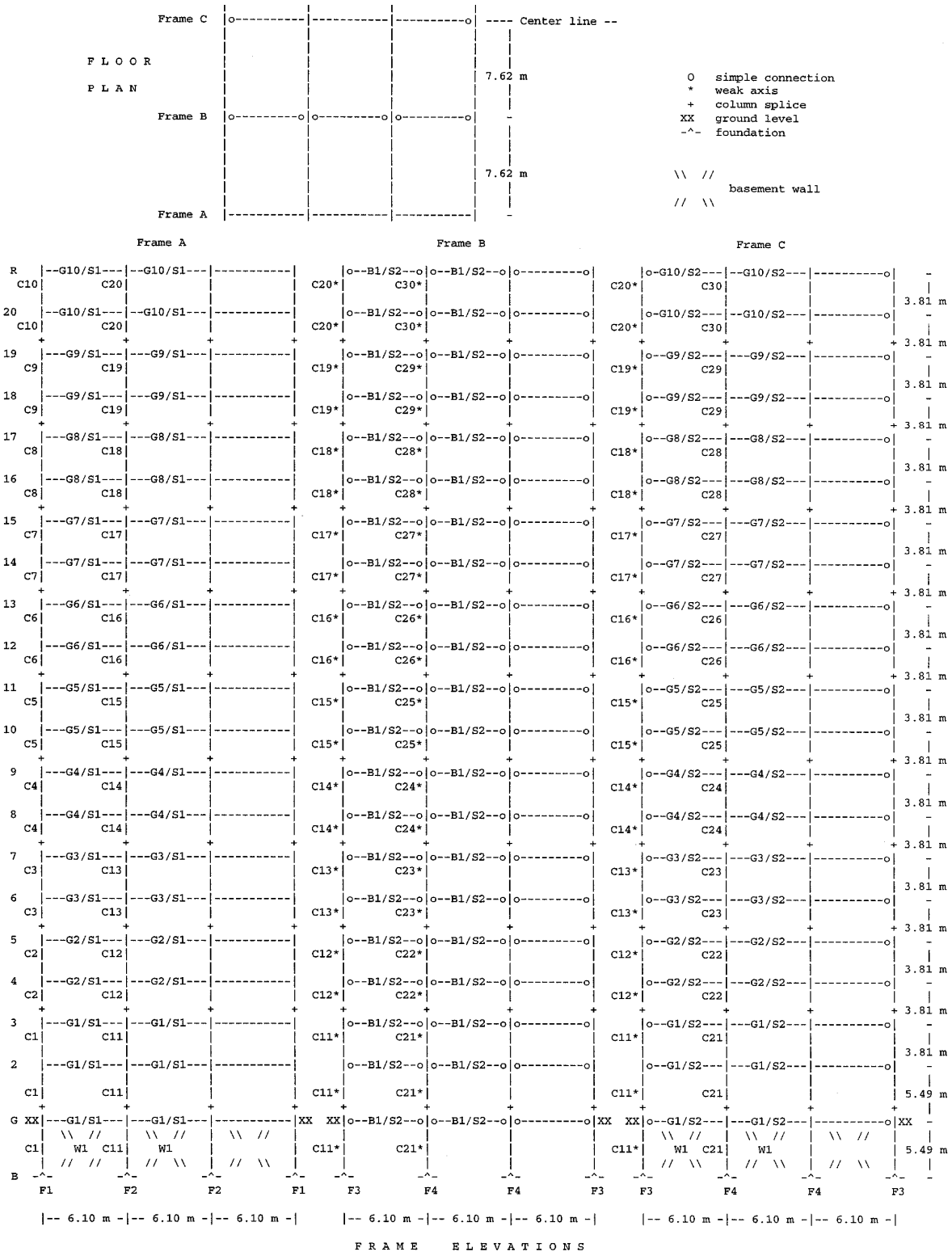

Figure 2.3: This twenty-story building (J20), designed to the 1992 JBC seismic provisions, is stiffer and stronger than the equivalent building designed to the 1994 UBC. Reproduced from Hall (1997).

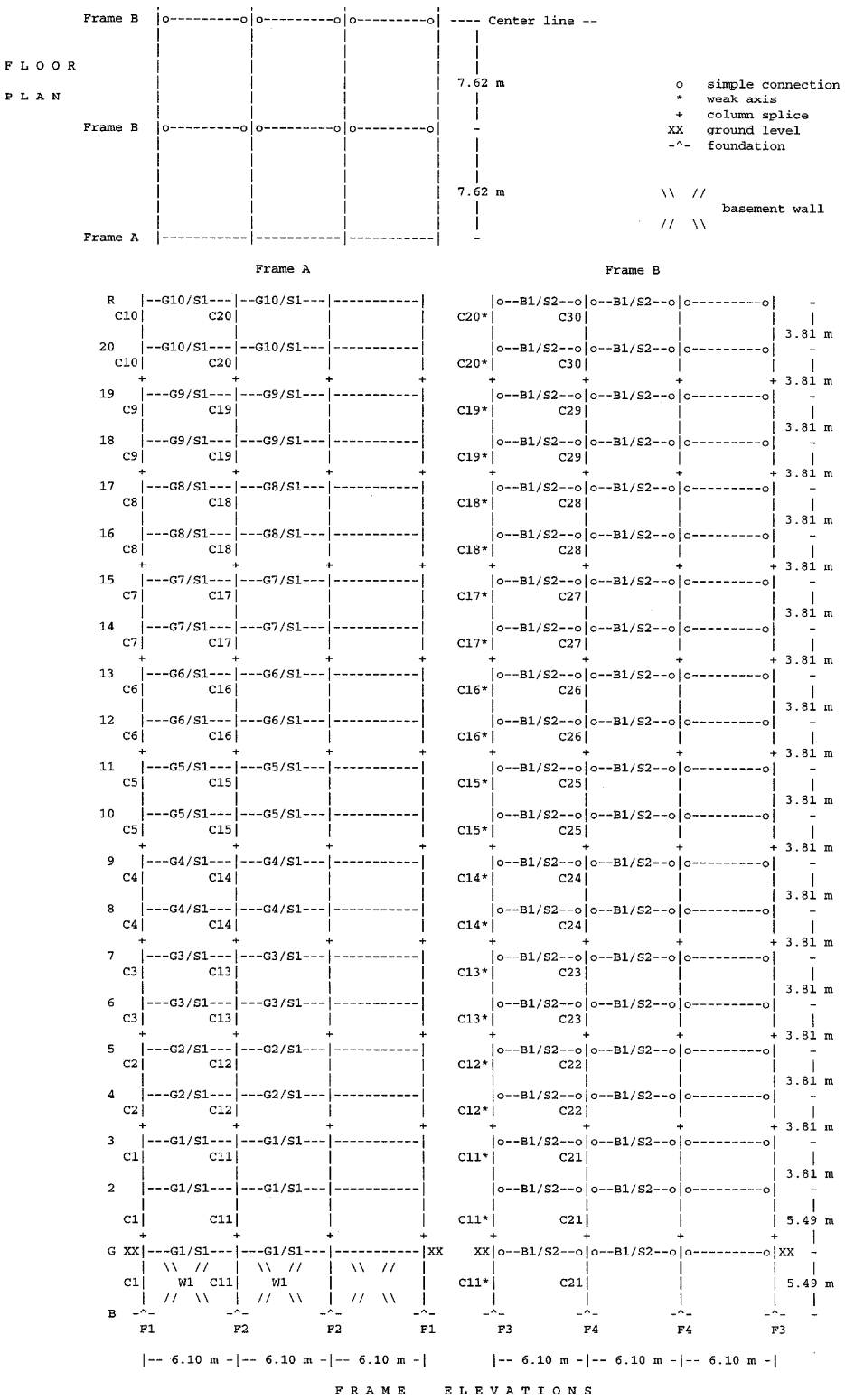

Figure 2.4: This twenty-story building (U20), designed to the 1994 UBC seismic provisions, is more flexible and has a lower-strength than the equivalent building designed to the 1992 JBC. Reproduced from Hall (1997).

Model	*Z*	*I*	R_W	*S*	*T*	*C*	*V/W*	*Drift limit*
U6	0.4	1	12	1.2	1.22 s	1.312	0.0437	0.25%
U20	0.4	1	12	1.2	2.91 s	0.736	0.0300	0.25%

Table 2.1: This table reports the values of 1994 UBC design parameters for the six- and twenty-story building designs. Reproduced from Hall (1997).

Model	*Z*	*Soil*	R_t	*T*	C_o	*Q/W*	*Drift limit*
J6	1	Type 2	0.990	0.73 s	0.2	0.1980	-
J20	1	Type 2	0.410	2.24 s	0.2	0.0820	0.50%

Table 2.2: This table reports the values of 1992 JBC design parameters for the six- and twenty-story building designs. Reproduced from Hall (1997).

2.1.1 Building Height

Building height affects the seismic response of steel MRFs. Existing steel MRF buildings can be generally categorized as short or tall, and the seismic responses of buildings at each height are different. In this thesis I simulate the responses of short and tall buildings with models that have six or twenty stories. For all buildings, the first floor height is 5.49 m, and the height of each upper story is 3.81 m. The basement height is 5.49 m. Thus the ground-to-roof height of the six-story buildings is 24.54 m and the height of the twenty-story buildings is 77.88 m.

2.1.2 Seismic Design Provisions

Hall (1997) designed the buildings to satisfy the seismic provisions of the 1992 JBC or the 1994 UBC. Tables 2.1 and 2.2 report the values of important design parameters.

The 1997 UBC adopted near-source factors to account for larger ground motions within 15 km of a fault due to directivity. The near-source factors at a site depend on the potential magnitudes and slip rates of local faults, as well as the distance between the fault and the site. The fault is categorized as type A, B, or C: type A faults have the potential to generate earthquakes of magnitudes greater than 7.0 and have a slip rate greater than 5 mm/year; type C faults have a magnitude potential less than 6.5 and have a slip rate less than 2 mm/year; and type B faults are those not characterized as type A or B. Most segments on the San Andreas fault are type

A, and most other faults in California are type B. Depending on the fault type and distance between the site and fault, the velocity-based near-source factor, N_v, ranges from 2.0 (sites within 2 km of the fault) to 1.0 (sites greater than 10 km to the fault). For example, in order to satisfy the 1997 UBC, a building designed in San Francisco within 10 km of the San Andreas would have a N_v of 1.2.

Hall (1998) compared the four building designs used in this thesis to the 1997 UBC seismic provisions. Lateral loads were applied to each design, according to the static lateral force procedure, until the stresses or drifts reached their allowed limits. The base shear at this limiting load was compared to the design base shear for each design. The six-story JBC design satisfies the 1997 UBC seismic provisions for all velocity-based near-source factors. The twenty-story JBC design satisfies only the least stringent near-source factor ($N_v = 1.2$). Neither the six-story or twenty-story UBC designs satisfies the 1997 UBC seismic provisions. Thus, the building responses of the JBC designs may be consistent with those of 1997 UBC designs for shorter buildings at all near-source sites and for taller buildings at sites with N_v less than or equal to 1.2.

Although the buildings were designed to the provisions of two specific building codes, I do not compare the two building codes themselves. The philosophy of the JBC is to promote stronger buildings that remain elastic in moderate earthquakes. The UBC philosophy promotes longer-period buildings which are less vulnerable in moderate, more frequent earthquakes. I compare the building designs as realizations of these philosophies instead of comparing the specific rules that generate specific buildings.

2.2 Finite Element Models

Since this thesis applies strong ground motions to steel MRFs, the building models must account for the deformation of such frames in large lateral loads. The finite element models are multi-degree-of-freedom frames with nonlinear, hysteretic material models and panel zone yielding. The finite element models account for the second-

order moments induced in columns that support eccentric vertical loads, or P-Δ effects. The following sections describe aspects of the finite element models that are pertinent to this thesis. Hall (1997) provides further details of the models, which are used in this thesis without modification.

2.2.1 Planar Frame Models

The building models are planar, and thus only produce planar responses. The buildings are rectangular in plan and have uniform mass and stiffness in plan as well. Since the centers of mass and rigidity are the same, a uniform ground motion at the base of the model cannot excite a torsional component in elastic response. Further, it is assumed that out-of-plane loading does not contribute to in-plane response. Since seismic ground motions have two horizontal components, a building deforms in the two horizontal directions by bending about the strong and weak axes of the columns simultaneously. The models in this thesis do not include torsional or out-of-plane responses.

The models explicitly define the beams, columns, joints, and basement walls of several frames to represent the buildings. Every model has an exterior frame with moment-resisting joints. The JBC models have an interior frame with simply-supported joints and a half interior frame with moment-resisting joints. (The half frame is due to explicitly modeling only half the building.) The UBC models have a single interior frame that represents one and a half frames with simply-supported joints. (The half is the contribution of the frame with simply-supported joints on the transverse centerline.) Rigid springs that represent the floor systems connect the frames.

Although the building models used in this thesis are planar, the building responses of three-dimensional models should be similar to those of planar models. Carlson (1999) compared the responses of two- and three-dimensional models of a seventeen-story steel moment resisting frame with a masonry service core. The author included the strength and stiffness contributions of the interior gravity frames in

both models. The author showed that the two- and three-dimensional building model responses did not differ significantly for most of the considered, recorded ground motions. For some simulations, however, the peak inter-story drift ratio (IDR, discussed in Section 2.4) of the three-dimensional building model was less than the peak IDR of the two-dimensional building model. Chi et al. (1998) modeled the same seventeen-story building with two- and three-dimensional building models as well. Their two-dimensional model, however, only included one exterior moment-resisting frame. A three-dimensional model connected the moment and gravity frames with a rigid floor system, and a second three-dimensional model used beam elements with rotational springs at the ends to model bolted shear plate connections. The authors applied strong ground motions recorded near the building in the 1994 Northridge earthquake to compare the recorded and simulated building responses. The peak IDRs in the two-dimensional models were approximately 2.5%, whereas the peak IDRs in the three-dimensional models were 1.2–1.3% (rigid floor and no core), 1.8–2.3% (rigid floor with core), and 1.3–1.6% (flexible floor with core). The present thesis considers only the responses of two-dimensional models of steel moment frame buildings. These studies suggest that the planar models capture most of the building response in strong ground motions. I expect a three-dimensional model of these building would predict similar, or slightly smaller, peak inter-story drifts compared to the planar model.

2.2.2 Fiber Method

The finite element models use the fiber method to discretize the buildings. This procedure subdivides the lengths of beams and columns into segments and further subdivides each segment cross section into fibers (Figure 2.5). Thus each beam or column has sixty-eight or eighty individual elements or fibers (eight segments times eight or ten fibers).

This method is distinct from the plastic hinge formulation. According to that discretization, a beam or column behaves as a single element with the capacity to form plastic hinges (or kinks) at the ends. Hall and Challa (1995) compared the responses

of twenty-story MRFs modeled with the plastic hinge or fiber element method. They applied a ramped, harmonic base excitation to the frames and found that the two models predict the rate of collapse onset and ductility demands consistently. However, the detailed responses of the two models before collapse differ. The plastic hinge model predicts somewhat larger lateral displacements of floors 2–5. The fiber element model develops an obvious, unrecovered lateral displacement before the plastic hinge model does. Consequently the fiber element model collapses before the plastic hinge model does.

For the purposes of this thesis, the advantage of the fiber method is the ability to model brittle welds. The behavior of each fiber can be specified independently, and fibers representing welded segments can thus have a fracture model. I describe specific weld fracture models in Section 2.2.7.

2.2.3 Beam and Column Elements

The beam and column elements have distinct material models for axial and shear deformations (Hall, 1997). Each fiber has a nonlinear, hysteretic, axial stress-strain model. Figure 2.6 shows the backbone curve of this model. The five user-defined parameters shown in this figure completely define the curve, which in turn defines the axial deformation behavior of the beam or column fibers. Table 2.3 lists the material model parameters and the values I use in this thesis. Each beam or column segment has linear shear stiffness in the plane of the frame. Tensile and compressive behaviors are the same.

The finite element models also account for residual stresses in the steel. The user defines a residual stress, and the model distributes that stress, as tensile or compressive, over the cross section of each segment. I use a residual stress of 6 ksi in the building models.

Two fibers of each beam segment model a deck-slab floor system. The concrete slab axial stress-strain material model is linearly elastic-perfectly plastic in compression and linear to a tensile crack stress. After cracking, the slab fiber no longer resists

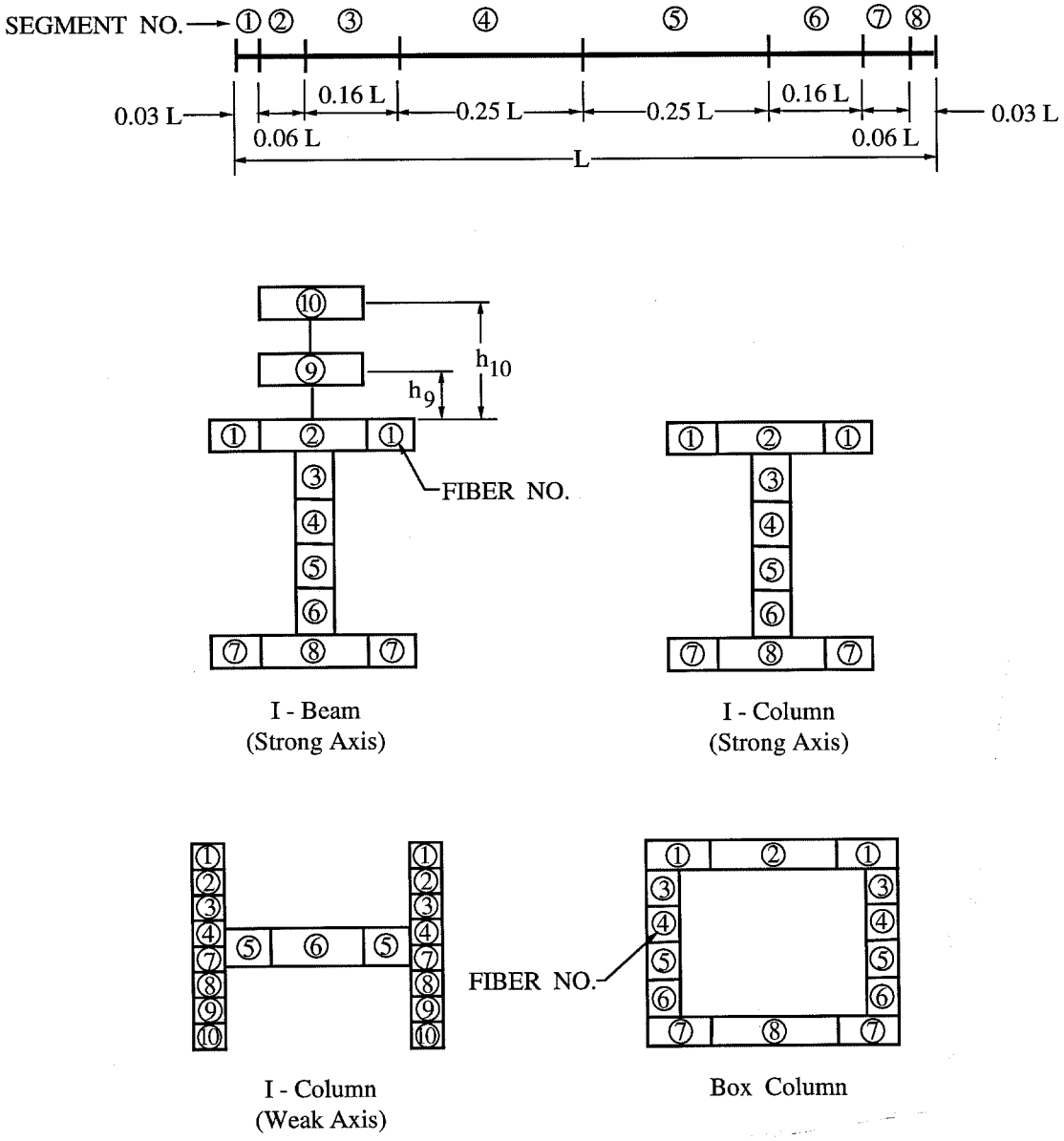

Figure 2.5: The finite element models of the four building designs use the fiber method. Each beam and column element is subdivided into eight segments on the length and into eight or ten fibers on the cross section. Fibers 1–8 represent the steel beam or column. Fibers 9 and 10 represent a deck-slab floor system. Reproduced from Hall (1997).

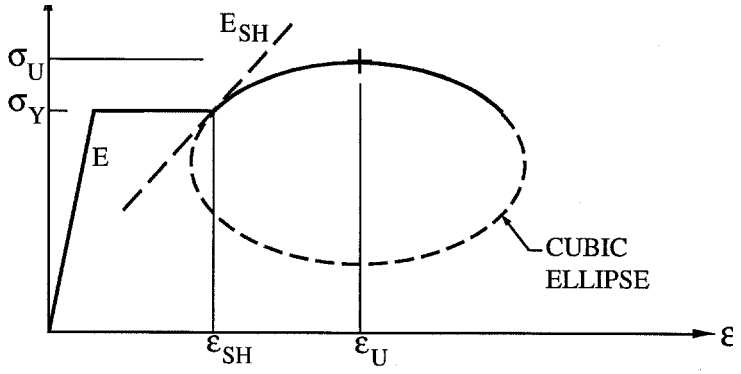

Figure 2.6: The axial stress-strain material model for each fiber is nonlinear and hysteretic. This curve defines the backbone shape for both tensile and compressive loading. Table 2.3 defines the parameters and their values. Reproduced from Hall (1997).

Parameter	*Symbol*	*Value*
Young's modulus	E	29,000 ksi
Initial strain hardening modulus	E_{SH}	580 ksi
Yield stress	σ_Y	42 ksi
Ultimate stress	σ_U	50 ksi
Strain at onset of strain hardening	ϵ_{SH}	0.012
Strain at ultimate stress	ϵ_U	0.16
Poisson's ratio	-	0.3

Table 2.3: These parameter values define the nonlinear, axial stress-strain behavior of the element fibers. This thesis does not consider alternate material models.

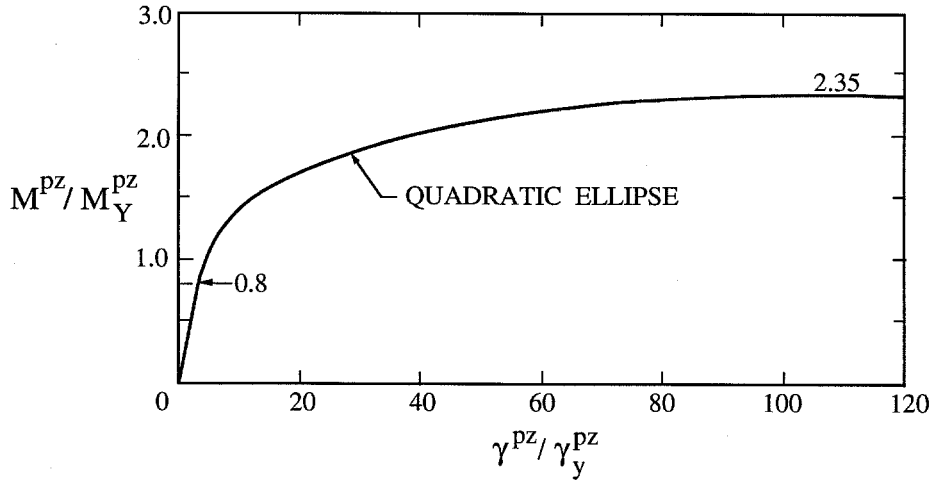

Figure 2.7: This backbone curve defines the nonlinear, hysteretic moment-shear strain relation of the panel zone element. M^{pz} is the magnitude of the double couple in the panel zone due to the moment and shear forces in the adjacent beams and columns, and γ^{pz} is the shear strain in the panel zone. Reproduced from Hall (1997).

tensile loading, but it can resist compressive loads if the crack closes.

2.2.4 Panel Zones

The finite element models include an element to explicitly model the deformation at beam-to-column joints, also known as panel zone behavior. This element models the moment versus shear strain behavior with a nonlinear, hysteretic relationship. Figure 2.7 defines this relation. In the finite element models the shear stress at yield, τ_Y, is 24 ksi, and the panel zone shear modulus, G^{pz}, is 11,6000 ksi. The panel zone yield moment, M_Y^{pz} in Figure 2.7, is 0.8 times the product of the panel zone volume and the shear stress at yield. The panel zone shear strain at yield, γ_Y^{pz}, is the shear stress at yield divided by the panel zone shear modulus.

In small ground motions, the beam-to-column joints remain rigid to ensure that the beams and columns deform in double curvature, as intended in a moment-resisting frame. In strong ground motions, however, panel zone yielding significantly and advantageously contributes to the steel MRF response. Challa and Hall (1994) identify two positive contributions of panel zone yielding in large ground motions: "First,

such panel zones reduce the ductility demands on the other structural elements by dissipating energy themselves. Second, being relatively weak, such panel zones act as fuses and limit the column moments, making it more difficult to form a collapse mechanism involving column hinges." Panel zone yielding is an important mechanism to include in MRF models that sustain large deformations.

2.2.5 Basement Walls and Soil-Structure Interaction

The finite element models of the four building designs include basement walls and soil-structure interaction. The wall elements have linear shear stiffness, but they do not resist rigid rotations. The wall elements also provide some linear, axial stiffness to the adjacent columns and beams. Soil-structure interaction is modeled with horizontal and vertical axial springs at the base of each column. The stress-strain relationship of the springs is bilinear and hysteretic.

This thesis uses a simple model of soil-structure interaction because it is adequate for the purposes of this thesis. Wong (1975), for example, studied several phenomena induced by the coupling of soils and structural foundations. The author developed sophisticated models to understand the physical behavior. Jennings and Bielak (1973) considered a simplification of the soil-structure interaction problem: they modeled the soil with an elastic half-space and the structure with an n-degree-of-freedom oscillator. The authors reformulated the problem as (n + 2) single-degree-of-freedom, viscously damped, elastic oscillators with rigid-base excitation and showed that all natural periods of the structure lengthen with soil interaction. The authors concluded that, for tall buildings, soil-structure interaction significantly affected only the fundamental period, and the effect was due to rocking of the structure rather than translation of the base. Stewart et al. (2003) compared the soil-structure interaction design procedures in the pre-2000 and 2000 *National Earthquake Hazards Reduction Program Recommended Provisions for Seismic Regulations for New Buildings and Other Structures*. The authors concluded that the effects of soil-structure interaction on long-period structures are negligible since the structure itself is so flexible. Thus,

this thesis uses a simple model to incorporate the main effect of soil-structure interaction (that is, a lengthening of the fundamental period of the building). However, I do not expect that including this interaction significantly affects the building responses.

2.2.6 Damping

The finite element models have light, viscous damping. One source is stiffness-proportional damping. This damping is 0.005 of the stiffness at the fundamental mode of the building model. This amount corresponds to the following fractions of critical damping for the four designs: 1.3% (J6), 0.98% (U6), 0.49% (J20), and 0.41% (U20). The second source of damping is inter-story shear damping. In addition to the stiffness of each column, there is a capped, viscous shear damper as well. The damping force is linear until the relative lateral velocities in adjacent floors reaches 0.1 m/s. For this and larger velocities, the damping force is a constant. This constant is found by applying the seismic design forces as a fraction of the design weight scaled by 0.02 (six-story designs) or 0.01 (twenty-story designs). The capped damping force constant is the resulting inter-story shear force.

2.2.7 Brittle Welds

In this study, the steel MRF finite element models may have fracture-prone or sound welds. Recall from Section 2.2.3 that each beam and column element is subdivided into eight segments along the length, and the cross section of each segment is subdivided into eight or ten fibers (Figure 2.5). Certain segments of beam and column elements represent welds. For all beams at a moment-resisting joint, the beam end segment represents a weld. The middle segment of some columns represents a welded column splice (see Figures 2.1–2.4 for locations), and the end segment of column elements at the foundation represents a column base plate weld. The fibers of the segments that represent welded connections each have a fracture strain. If the axial strain in a fiber exceeds the fracture strain, then that fiber no longer resists tensile loads. The fiber can continue to resist compressive loads as usual if it re-establishes

contact.

The fracture strain may not be the same for all fibers in a segment that represents a weld. For beams, the top fibers (fibers 1–4 in Figure 2.5) represent the weld between the beam top flange and the column flange, and the bottom fibers (fibers 5–8 in Figure 2.5) represent the weld between the beam bottom flange and the column flange. The finite element model allows different definitions of the fiber fracture strains for the two welds, or groups of fibers. All fibers of the column splice and base plate segments represent a single weld, and thus all fibers in those segments have the same fracture strain.

The finite element model randomly assigns a fracture strain to a weld from a user-defined distribution of fracture strains. Figure 2.8 shows two such distributions, called "B" and "F" welds from Hall (1997) and Hall (1998), respectively. The finite element model samples the fracture strain for each beam top flange, column splice, and column base plate weld from one distribution at the top of Figure 2.8. Similarly, the model samples the fracture strain of each beam bottom flange weld from one distribution at the bottom of Figure 2.8. For example, the finite element model randomly chooses a fracture strain for a column splice weld from the B weld distribution of possible column splice fracture strains (top of Figure 2.8). This sampling repeats for all welds. After this assignment completes, the distribution of all assigned fracture strains should resemble the user-defined distribution. In statistical jargon, the sampled distribution should resemble the population distribution.

The B and F weld fracture strain distributions are two models of brittle weld failure. The B distributions are bimodal: there are either relatively low or high fracture strains, but no moderate fracture strains. The F weld distribution is more uniform at the moderate fracture strains. There is no empirical evidence to recommend one distribution is better than the other. In Section 2.7.3 I compare the simulated responses of models with B or F weld distributions. For all other sections of this thesis, I use the B weld distribution to model buildings with brittle welds. I denote buildings with sound, or perfect, welds with P.

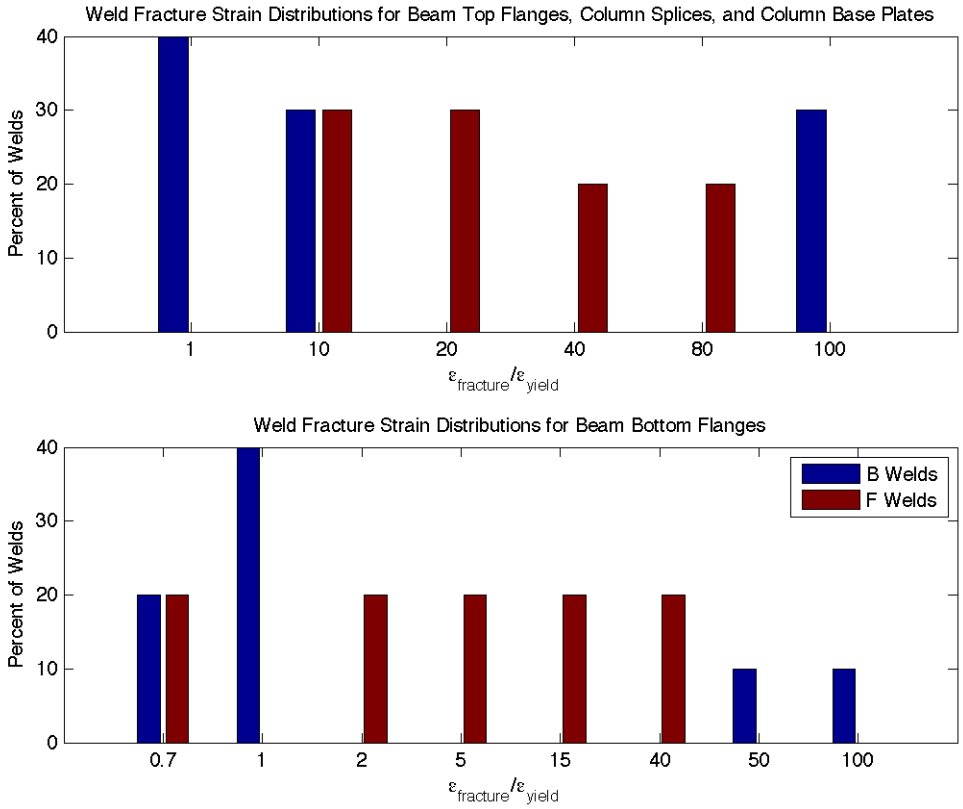

Figure 2.8: For models with brittle welds, the finite element model randomly samples a weld fracture strain from a user-defined fracture strain distribution. This thesis considers two such distributions: B and F welds.

	Modal Periods [s]	
Model	*First*	*Second*
J6P	1.2	0.4
J20P	3.2	0.9
U6P	1.6	0.5
U20P	3.8	1.0

Table 2.4: The modal periods indicate what energy content in ground motions amplify the building response through resonance. Thus, ground motions should have energy content for periods at least equal to and greater than the first mode period.

2.3 Characterization of Building Models

The preceding sections describe the components of the nonlinear finite element models, and the following sections describe the building models as systems of those components. I report the undamped, first and second modal periods and characterize the flexibility and strength of the building models by performing pseudo-static pushover analyses. The simulated ground motions used in this thesis are primarily near-source, and so I discuss the deformed shape and collapse mechanism of steel MRFs in strong ground motions.

2.3.1 Elastic Periods

One characterization of a building is its modal periods. Figure 2.9 shows the frequency response of the four, undamped building models. There is significant amplification of the harmonic building response near the first modal period. Table 2.4 reports the elastic first and second mode periods without the viscous damping described in Section 2.2.6. The second mode periods are approximately one-third of the first mode periods, which is predicted by the shear beam model of a building. The building response at the first modal period dominates the resonance behavior. Ground motions with significant energy at the first modal period amplify the building response compared to ground motions with energy at other periods.

There are two characteristic types of ground motions in the set assembled for this thesis. The first type is dominated by a near-source directivity pulse in displacement

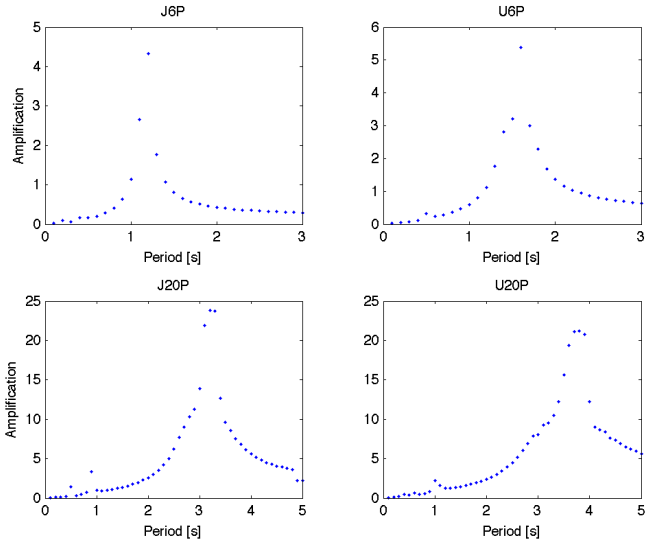

Figure 2.9: The frequency response of the building models provide one characterization of the models. Amplification refers to the amplitude of steady state roof displacement divided by the amplitude of the excitation.

and velocity. If the period of this pulse is approximately the fundamental period of a building, then the pulse induces a large, transient resonance amplification. Hall et al. (1995) describe the building response in such a pulse: as the ground moves forward, the base of the building follows the ground while the top lags. When the pulse reverses direction, the top has forward momentum while the base begins to move in the backward direction. The top moving forward as the base moves backward causes shear deformations, especially in the lower stories.

The second type of ground motions in this set are characterized by amplification of surface waves in sedimentary basins. This trapping of long-period energy in basins results in long-duration, primarily harmonic ground motions. If the dominant period of these ground motions is approximately the fundamental period of a building, the building will experience steady-state resonance, and the amplified, long-duration excitation leads to large building responses as well.

Figures 2.10 and 2.11 report the peak IDRs of twenty- and six-story buildings by story. For twenty-story buildings, primarily stories 2–4 collapse (that is, peak IDR exceeds 10%), and for six-story buildings, the collapses (peak IDR exceeds 16%)

happen mostly in stories 1–3. For buildings that do not collapse, the peak IDR can happen in the upper stories, but it is much more likely that the peak IDR is in the lowest stories.

The energy content of simulated ground motions affects how they can be used. Deterministic ground motion models provide accurate predictions of long-period content. The short-period content is not well understood, but stochastic ground motion models exist to include energy at short periods (for example, Graves and Pitarka (2004)). Thus not all simulated ground motions can be used in all applications. Long-period ground motions are not adequate to predict the response of buildings sensitive to short-period energy. However, it is appropriate to apply long-period ground motions to a building with a long fundamental period. In this thesis I apply long-period ground motions (energy content greater than 2 s) to buildings with a fundamental period longer than 2 s, and I apply broadband ground motions (energy content greater than 0.1 s) to all building models.

2.3.2 Pushover Curves

Another way to characterize building response is with a pushover curve. A pushover curve relates the shear in the ground floor columns (base shear) to the lateral roof displacement for increasing lateral loads. To generate the curves I apply a slowly increasing, pseudo-static, lateral load to each model. The load must increase slowly enough so inertial and damping forces do not contribute to the base shear. The lateral load is distributed vertically in proportion to the lateral design loads. Figures 2.12 and 2.13 show the pushover curves for the eight building models in this thesis.

The curves show three important characteristics of the buildings: stiffness, base shear at yield, and ductility. The stiffness is the initial slope of the pushover curves. I use this characteristic to compare the models, rather than as an absolute value. That is, a model is "stiffer" or "more flexible." The base shear at yield is one measure of the building's strength. Similar to stiffness, I use building strength to compare designs

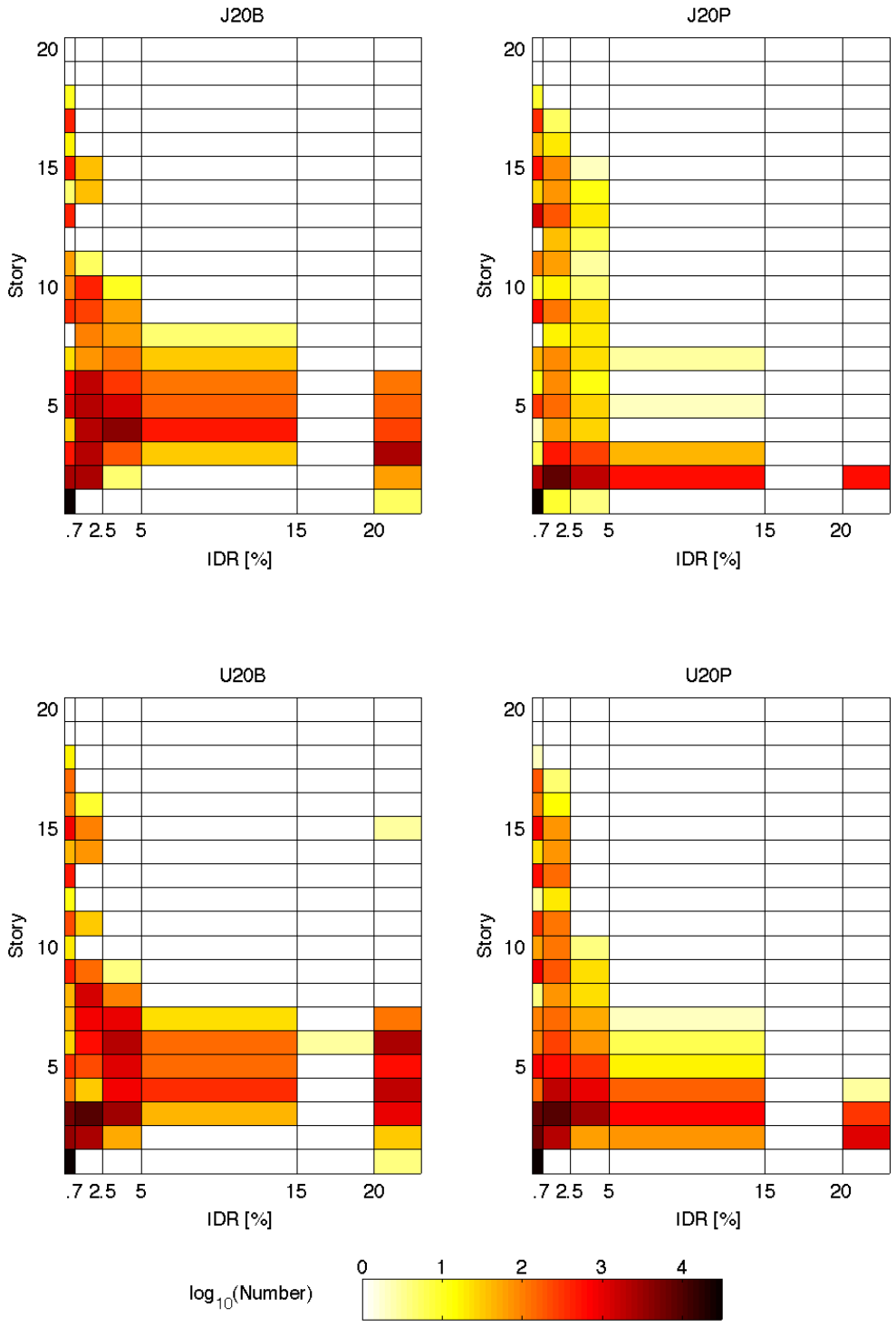

Figure 2.10: For twenty-story buildings, this figure disaggregates the peak IDR by story, or in other words, shows in what story the peak IDR occurred. Models that collapse in the simulations (peak IDR greater than 10%) develop peak drifts in the first six or seven stories. The building models can develop small peak IDRs in the first eighteen stories.

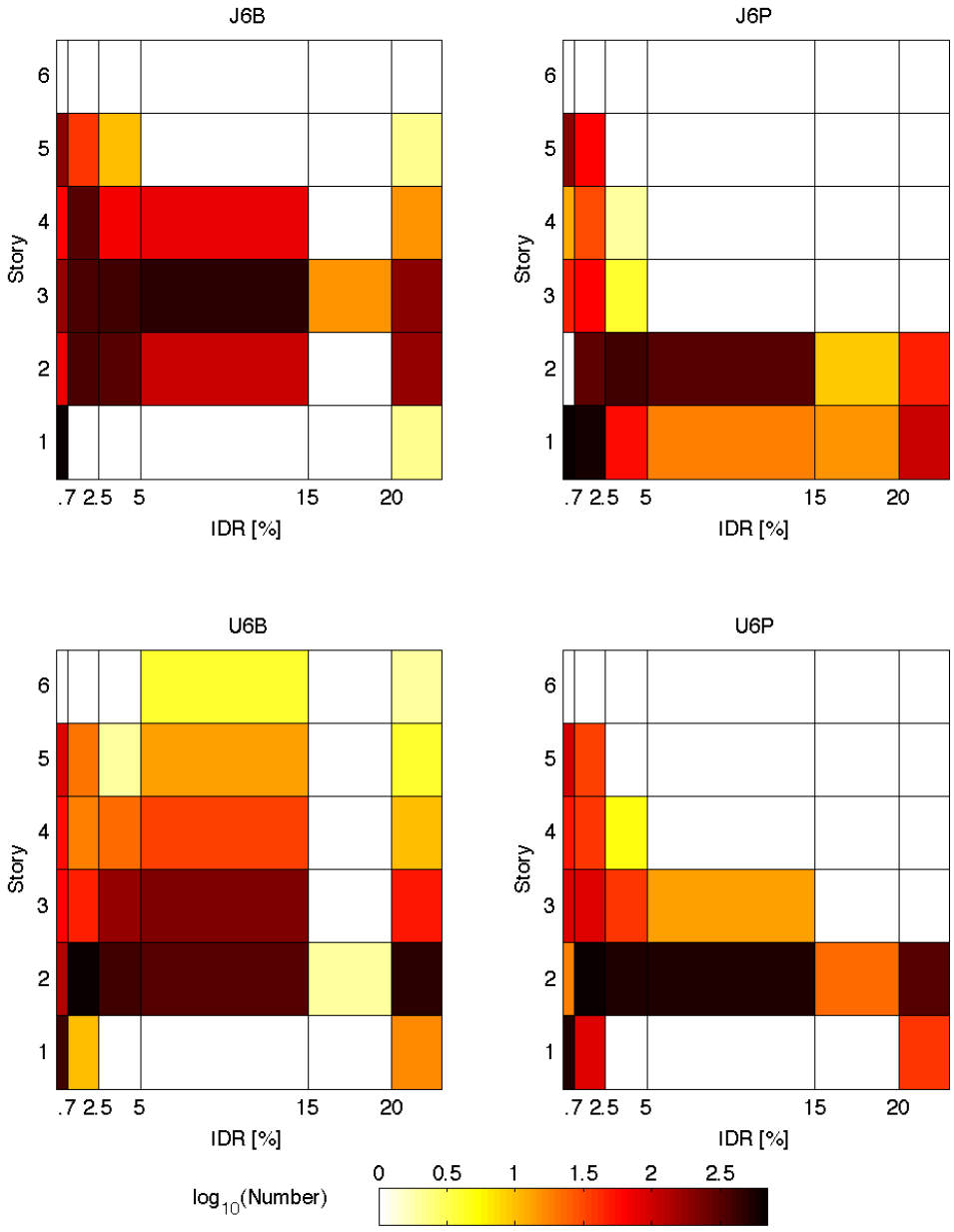

Figure 2.11: For the six-story buildings, this figure disaggregates the peak IDR by story. Models that collapse (that is, with a peak IDR greater than 16%) tend to do so in the first four stories. Small peak IDRs develop in any of the first five stories.

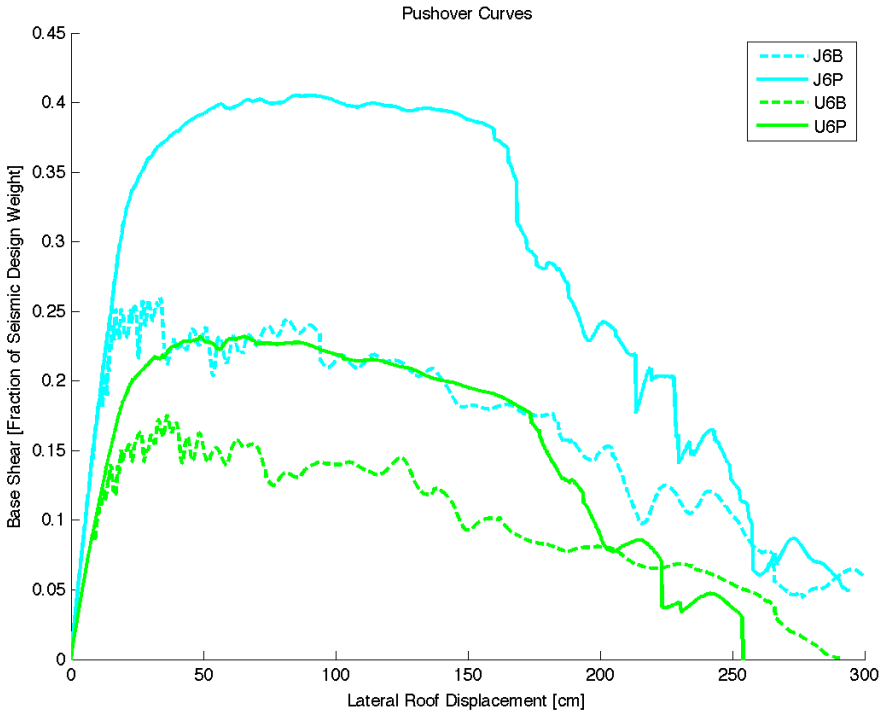

Figure 2.12: This figure shows the pushover curves for the six-story building models.

as higher- or lower-strength. A building's ductility is the ratio of the displacement after which the base shear drops precipitously to the displacement at yield. Ductility indicates the relative amount of deformation that a building can sustain after it has yielded. Note that the ductilities of the building models are similar for the JBC and UBC designs.

2.4 Measurement of Building Responses

Researchers and practitioners use various measurements of building response, depending on the response they want to characterize. One engineer may be interested in the behavior of individual beams, columns, or joints. Another may study a few critical members for the onset and progress of yielding or for the physics of collapse. On a larger scale an engineer may want to characterize the response of entire floors or the building as a whole. Each of these studies requires a different measure of building

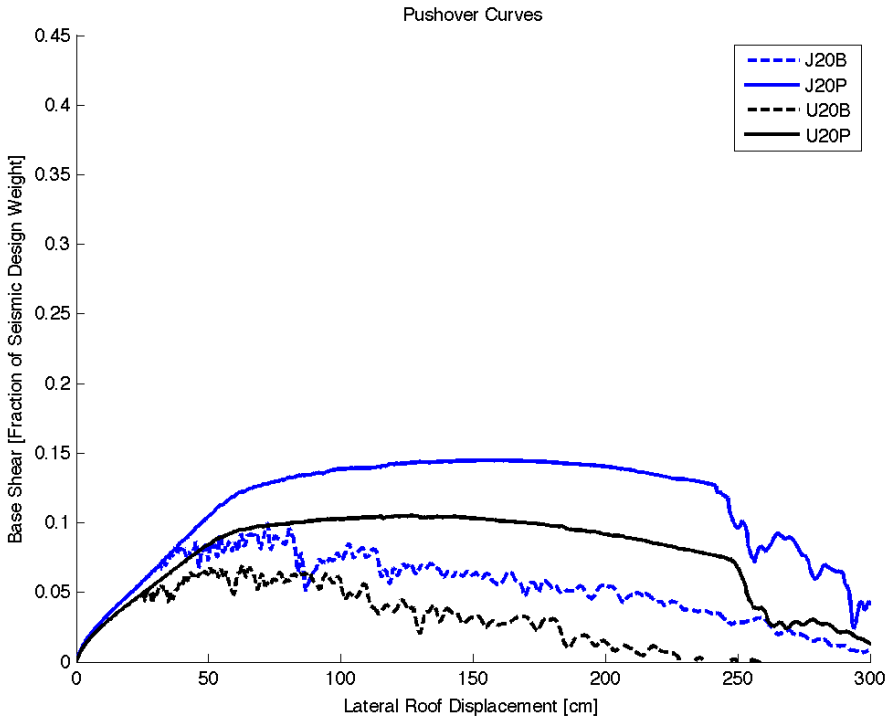

Figure 2.13: This figure shows the pushover curves for the twenty-story steel moment frame building models.

response, appropriate to the level of detail under consideration.

Due to the large number of building responses, I measure overall building performance. One measure is peak dynamic inter-story drift ratio. The inter-story drift ratio quantifies the amount of shear deformation within a story by expressing the relative lateral displacement of two floors as a ratio of the story height. The largest such ratio for all stories and for all time steps in the ground motion time history is the peak IDR.

The peak IDR is a common measure of building response. For example, FEMA 356 uses peak IDR to categorize building response: if the peak IDR is less than 0.007, the building is safe for "immediate occupancy" (American Society of Civil Engineers, 2000). If the peak IDR exceeds 0.025, the building state threatens "life safety." For peak IDRs greater than 0.05, FEMA 356 considers the response a "collapse." These numbers are guidelines to characterize states of building damage based on a quantifiable parameter; they represent a judgement of what the peak IDR would have been during the earthquake in order to produce the post-earthquake damage.

The second response measure is collapse, a categorical description. For the models I consider, collapse refers to the loss of all lateral load-resisting capacity. The finite element program I use does not model the physical collapse of the building; it does not account for some important deterioration mechanisms known to cause collapse in real buildings. Rather, I assume the loss of lateral resistance when the simulation shows unrealistically large deformations. No six-story building model shows reasonable deformations for peak IDRs greater than 0.16, whereas no twenty-story model has reasonable deformations with peak IDRs greater than 0.10 (Figure 4.5). Thus, as a practical matter, I terminate the simulation when the peak IDR reaches 0.2 (for computational efficiency) and deem the model response a collapse. Note that defining collapse as implausibly large deformations in the simulation differs from the definition in FEMA 356.

The third building response measure describes whether the building is a total structural loss, another categorical description. If a building does not collapse in a given ground motion, it may still develop a permanent lateral deformation that

cannot be repaired. In this case, the building is deemed a total structural loss and demolished. I measure this state by calculating the permanent drift over the ground-to-roof building height. If the ratio of the permanent total drift to the building height exceeds 0.0091, then the building is a total structural loss (Iwata et al., 2006). In this way, the three measures of building response (collapse, total structural loss, and peak IDR) characterize three important, permanent or transient, building states.

2.5 Broadband versus Long-Period Peak Ground Measures

This thesis collects and employs both broadband and long-period ground motions. The broadband ground motions have energy content for periods longer than 0.1 s, and the long-period ground motions have energy content for periods longer than 2 s. The peak ground displacement and velocity of a broadband ground motion are different for the same ground motion filtered for long-periods. For most ground motions, the peak ground displacement and velocity of the broadband ground motion are larger than those of the equivalent long-period ground motion.

This thesis measures the peak ground displacement and velocity for both broadband and long-period ground motions. I denote the peak ground displacement and velocity of a broadband ground motion as $\mathrm{PGD_{bb}}$ and $\mathrm{PGV_{bb}}$, respectively. Similarly, I abbreviate the peak ground displacement and velocity of a long-period ground motion with $\mathrm{PGD_{lp}}$ and $\mathrm{PGV_{lp}}$. If there is no distinction between the broadband and long-period peak ground measures, then I use peak ground displacement and peak ground velocity in a general sense.

2.6 Forms of Building Response Figures

This thesis presents maps of peak IDR. The maps report the response of a single building model at all sites in the simulation domain. No city is uniformly built

with steel MRFs, and thus the maps do not predict patterns of responses for the metropolitan areas as built. Rather, presenting the data in this manner highlights areas of large responses for each building model and indicates the areal extent of large building responses.

In addition to the maps, I graph the simulation results as functions of a ground motion intensity measure. The purpose of these graphs is to understand the building deformation as a response to the ground motion. Many intensity measures could characterize the ground motion time histories. I consider peak ground displacement (PGD), peak ground velocity (PGV), and pseudo spectral velocity ($PSV = \omega SD$, where ω is the fundamental circular frequency and SD is spectral displacement) as possible characterizations of the ground motions. Figure 2.14 graphs the peak IDR as a function of each intensity measure. There is more scatter in peak IDR as a function of PGD than as a function of PGV. The scatter in peak IDR varies with PSV: as PSV increases so does the scatter in peak IDR. For elastic building responses, PSV predicts peak IDR well because PSV filters the ground motion at the fundamental period of the building. For inelastic building responses, however, PSV no longer predicts peak IDR well because inelastic building behavior is not well characterized by the elastic response. The scatter in peak IDR for larger PSV is as large as—if not larger than—the scatter in peak IDR as a function of PGV. PGV is a more broadband measure of ground motion than PSV. Since this thesis studies building response in strong ground motions, PGV is a better intensity measure than PGD or PSV.

In all graphs of building response, I show the building state (that is, collapse or total structural loss) and peak IDR on two plots, one above the other. For some figures, the top plot reports the proportion of sites on which the model collapses or is a total structural loss for a given PGV value. The bottom plot reports the normalized peak IDR if the building stands. I normalize the peak IDR by removing the linear trend, which can be seen in Figure 2.14. For example, Figure 2.16 compares building responses in different orientations with respect to the horizontal ground motions. For a $\mathrm{PGV_{bb}}$ of approximately 3 m/s, buildings oriented at an angle, θ, equal to 60 deg collapse on 40% of the sites in the simulation domain. If the building stands or is

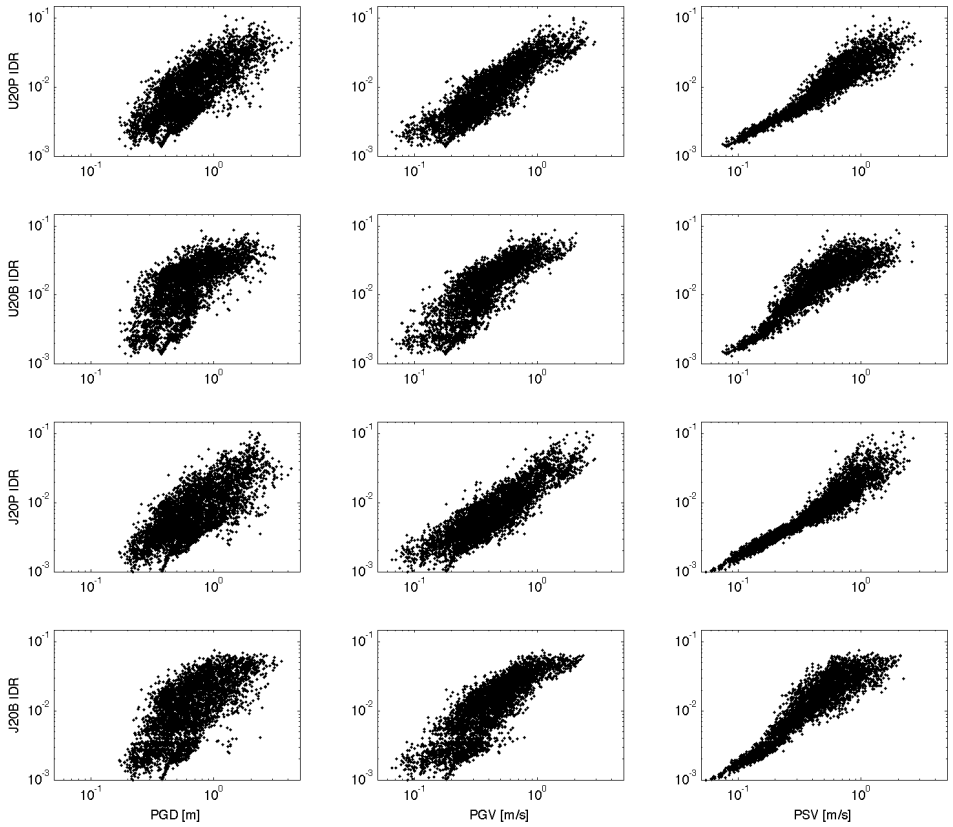

Figure 2.14: The remainder of this chapter, as well as Chapters 3–5, compare building responses as functions of a ground motion intensity measure. This figure motivates the choice of PGV as the intensity measure in these chapters. (Collapsed buildings are not represented in these plots.) PGD, PGV, and pseudo-spectral velocity (PSV; or similarly, spectral displacement or spectral acceleration) have an approximately linear relationship with peak inter-story drift ratio. The variance in peak IDR is smaller as a function of PGV compared to that from PGD. For PSV less than 0.2 m/s, the variance is quite small, however for larger PSV, the variance is larger. For large ground motions, the variance is larger for peak IDR as a function of PSV than for peak IDR as a function of PGV. Chapter 6 compares quantitatively building response prediction models based on PGD, PGV, and pseudo-spectral acceleration.

repairable at this PGV, then the range of peak IDR could be 0.3–3 times the median peak IDR.

Other figures compare two building responses at each site in the simulation domain. That is, the same ground motion is applied to two building models, and the building responses are compared directly. In these figures, the top plot has two lines, representing the proportion of sites where either of the two buildings collapses or is a total structural loss. The bottom plot reports the ratio of the peak IDR in one building to the peak IDR in the second, assuming both buildings stand or are repairable at the site.

2.7 Modeling Assumptions

To generate the responses of steel MRF buildings at so many sites for so many simulated earthquakes, I make several initial decisions about the modeling procedure. These choices include: how to combine the horizontal ground motions into a single resultant; whether to include the vertical component of ground motion; the distribution of weld fracture strain; and the seed number that generates the random assignment of fracture strain to individual welds. The following sections describe these choices and evaluate the effect of each choice on the results. Only the choices of how to resolve the two horizontal components of ground motion and of weld fracture strain distribution noticeably affect the building responses. The chosen horizontal resultant produces larger building responses for the same ground motion than other possible resultants. The chosen weld fracture strain distribution produces smaller building responses for the same ground motion, compared to an alternate distribution.

2.7.1 Horizontal Ground Motions

There is no standard way to apply two-component horizontal ground motions to buildings. The orientation of an existing building site is known with respect to a specific fault, so the horizontal components of ground motion can be properly applied in this case. This thesis, however, considers buildings at all sites in two broad geographic

regions (that is, the San Francisco and Los Angeles metropolitan areas). The orientation of a rectangular-plan building with respect to predicted ground motions is unknown at all sites. The streets in west Los Angeles, for example, run predominantly north-south (NS) and east-west (EW), but the longitudinal axis of a rectangular-plan building may be NS or EW. A building set at an angle with respect to the regular street grid, maybe for aesthetic reasons, would further complicate this issue. As a second example, the streets in Santa Monica are rotated approximately 45 deg from North. It is impractical to assign the most likely orientation of a rectangular-plan building at all 13,754 sites in the four simulation domains I consider.

I choose a particular orientation of the building models with respect to the ground motions based on the building response. I want to characterize the most damaging building response for a given ground motion. Further, the planar building models require a single horizontal component of ground motion and a single vertical component. I combine the two horizontal components to produce a single horizontal resultant that represents the most damaging orientation of a building with respect to the given ground motion.

Peak-to-peak velocity (V_{pp}) is a good measure of ground motion for predicting the response of steel MRF buildings, since a large forward-and-back pulse in displacement induces large drifts in the lowest stories. I orient the short dimension of the building models in the direction of the largest peak-to-peak velocity. I find this direction by combining the orthogonal NS and EW components at angles of 0 to 179 deg in increments of 1 deg (equation 2.1), producing 180 resultant horizontal ground motions. I select the resultant with the largest peak-to-peak velocity and apply that ground motion to building models at the site associated with the original NS and EW components. This angle is not the same for all sites in the simulation domain nor for all simulations on the same domain, so the buildings are not uniformly oriented with respect to North.

$$\text{Resultant}(t) = [\text{EW component}(t)] \cos\theta + [\text{NS component}(t)] \sin\theta \qquad (2.1)$$

The building response in the short dimension should be smaller than that in the long dimension. The design for wind loads requires more lateral force resistance in the short dimension due to the larger building surface area in the long dimension. Thus the building design is stiffer in the short dimension, resulting in smaller responses. By aligning the short dimension of the building with the largest peak-to-peak velocity, the resulting building responses should be relatively large for the given three-component ground motion but not the largest possible. If the long dimension of the building aligned with the largest peak-to-peak velocity, then the building response would be larger than the responses predicted in this thesis.

I evaluate the effect of choosing the resultant with the largest peak-to-peak velocity by comparing the building responses in several alternate horizontal resultants. The ground motions are from a magnitude 7.15 simulation on the Puente Hills fault in the Los Angeles basin. I combine the two horizontal components at angles of 0 to 150 deg in increments of 30 deg at all sites. This exercise produces six distinct ground motions at each site, including the pure EW ($\theta = 0$ deg) and NS ($\theta = 90$ deg) components. I compare the building responses to these six resultants and to the resultant with the largest peak-to-peak velocity.

Figure 2.15 maps the peak IDRs of the twenty-story, more flexible model with perfect welds (U20P) for six of the seven combinations. The resultants from angles of 0 (EW) and 150 deg induce large peak IDRs on small areal extents, compared to the other resultants. The pure NS component and the resultant with the largest peak-to-peak velocity induce large peak IDRs on the largest areal extents. Figure 2.16 graphs the simulated responses as a function of PGV_{bb}, which is independent of the combination of the two horizontal components. Resultants from angles of 30, 60, and 90 deg, and the largest peak-to-peak resultant cause collapse of the building on a larger proportion of sites for a given PGV_{bb} than do the other resultants. The largest peak-to-peak velocity resultant consistently produces the highest proportions of collapse. If the building remains standing, the peak IDRs are larger for resultant ground motions at these angles compared to the other angles. As desired, applying the horizontal resultant with the largest peak-to-peak velocity induces building responses

larger than those from other resultants.

I also find the resultant that maximizes peak-to-peak velocity by three algorithms. The three algorithms first combine the horizontal components at every angle from 0 to 179 deg in increments of 1 deg, generating 180 resultants. After this, the algorithms are distinct. The first algorithm finds the extrema in each resultant, determines the largest difference between consecutive extrema, and then finds the maximum difference over all resultants. This algorithm is not robust: for example, it cannot distinguish between consecutive maxima in the resultant. However, by inspection of dozens of the resultants, this algorithm consistently chooses the obviously large peak-to-peak velocity. The second algorithm measures the long period pulse, characteristic of near-source ground motions. This algorithm filters each resultant with a low-pass, Butterworth filter with a corner period of 2.5 s. Since the filter removes short-period content, the long-period pulse remains, albeit slightly attenuated. Since the purpose of the algorithm is not to find the value of the largest peak-to-peak velocity, but rather which resultant has the largest value, the amount of attenuation is not important. This method is robust because the filtered resultants have consecutive extrema that are peak positive and peak negative. The third method is the simplest: it calculates the distance between the most positive velocity and the most negative velocity over the entire unfiltered ground motion time history.

Figures 2.17 and 2.18 compare the peak IDRs for the twenty-story, more flexible building models with prefect welds (U20P) subject to the ground motions from each peak-to-peak velocity algorithm. The algorithm does not significantly affect the building response to the ground motion at the sites in the simulation domain. This study uses the first algorithm to select the combination of the two horizontal components that maximizes the peak-to-peak velocity. For computational efficiency, however, the difference between the peak positive and peak negative velocities (algorithm 3) can be used in place of the true peak-to-peak velocity (algorithm 1).

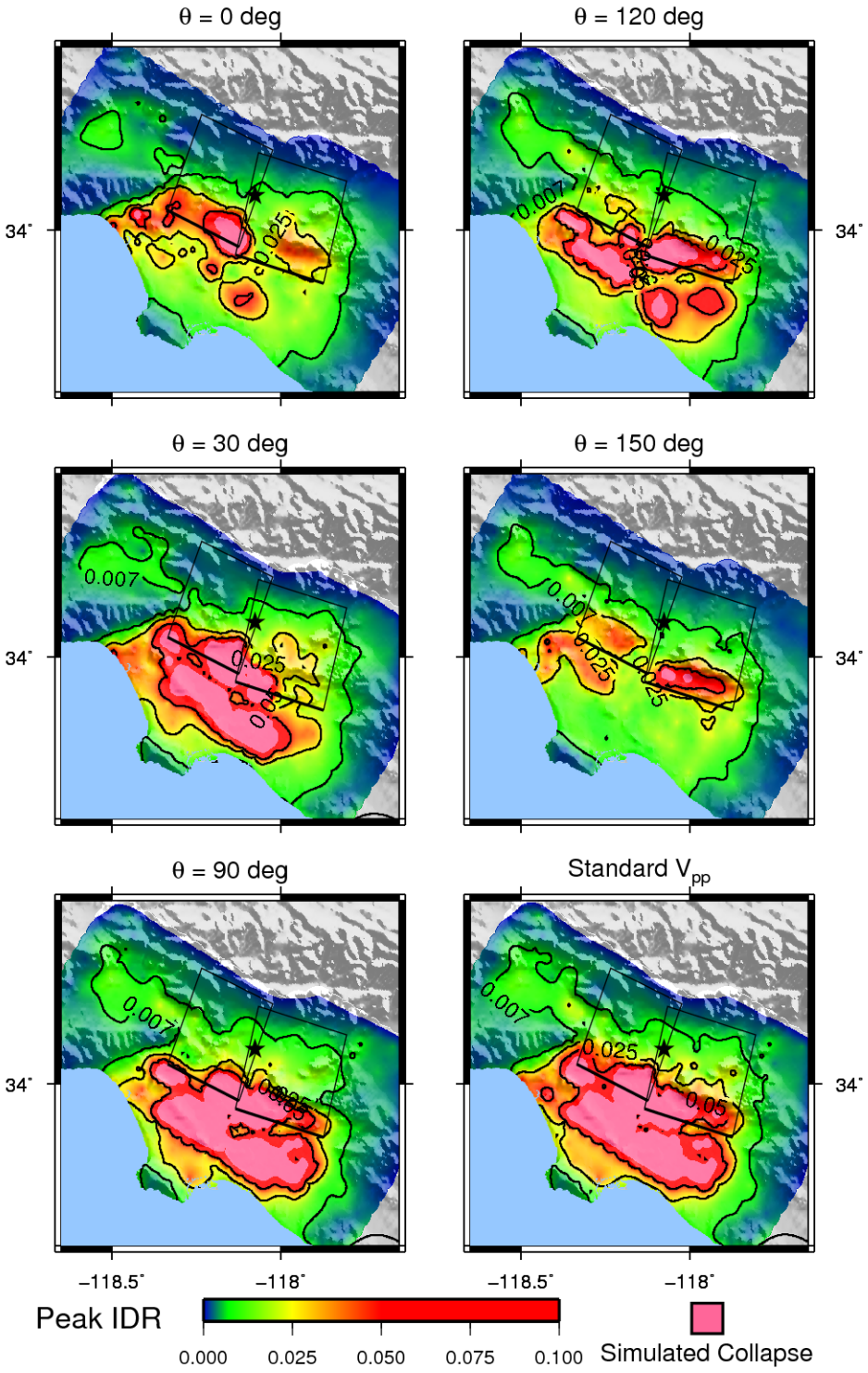

Figure 2.15: This figure maps U20P building responses to ground motions with various combinations of the horizontal components. For this simulation on the Puente Hills fault, the EW component (0 deg) induces smaller U20P building responses at a given site than does the NS component (90 deg). As desired, the resultant with the largest peak-to-peak velocity causes the largest building responses for each site on the simulation domain.

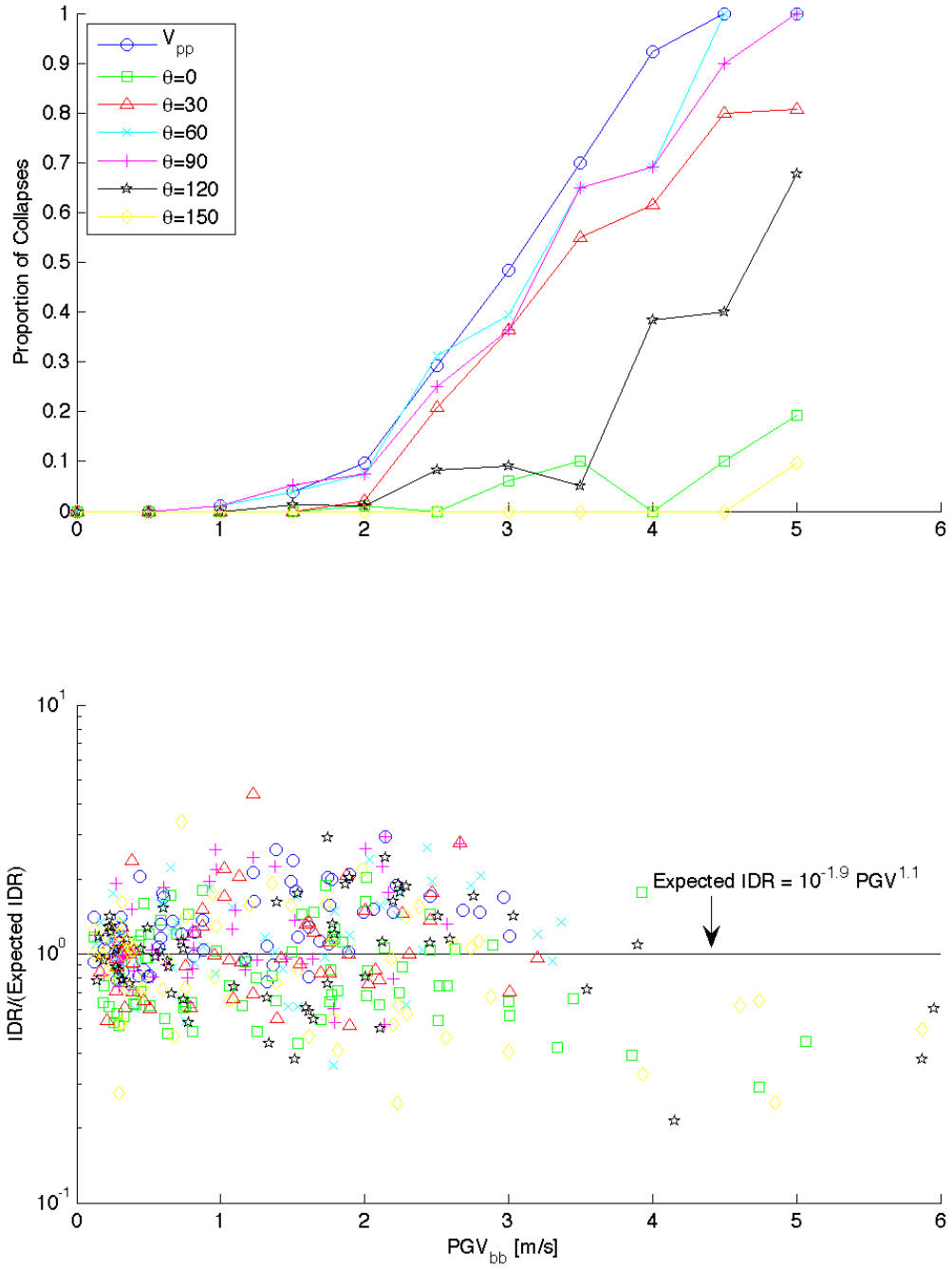

Figure 2.16: This figure compares the U20P building responses to several combinations of the horizontal component of ground motion. The resultant with the largest peak-to-peak velocity induces more collapses for a given PGV_{bb}. If the models do not collapse, the resultant with the largest peak-to-peak velocity also tends to induce larger peak IDRs than do the resultants from a single angle at all sites.

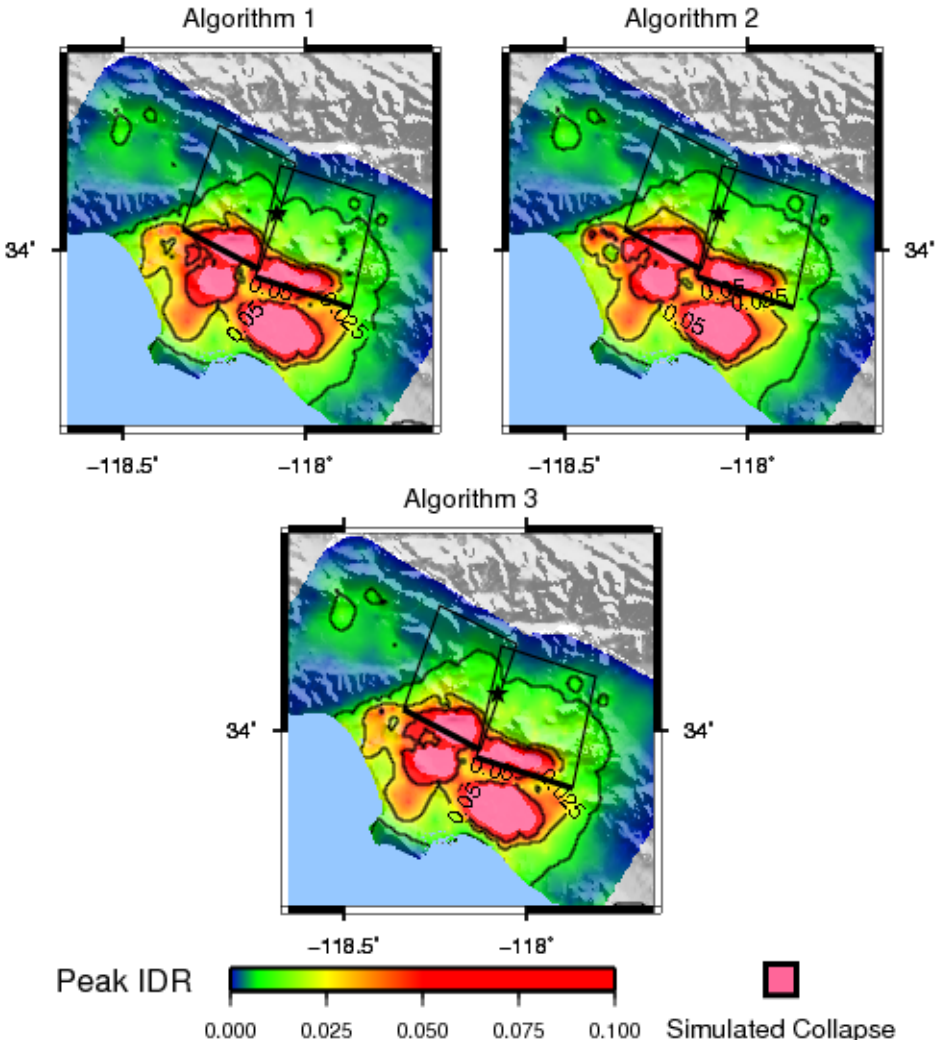

Figure 2.17: This figure compares U20P responses to resultant horizontal ground motions chosen by 3 peak-to-peak velocity algorithms. There are no apparent differences due to the peak-to-peak velocity algorithm.

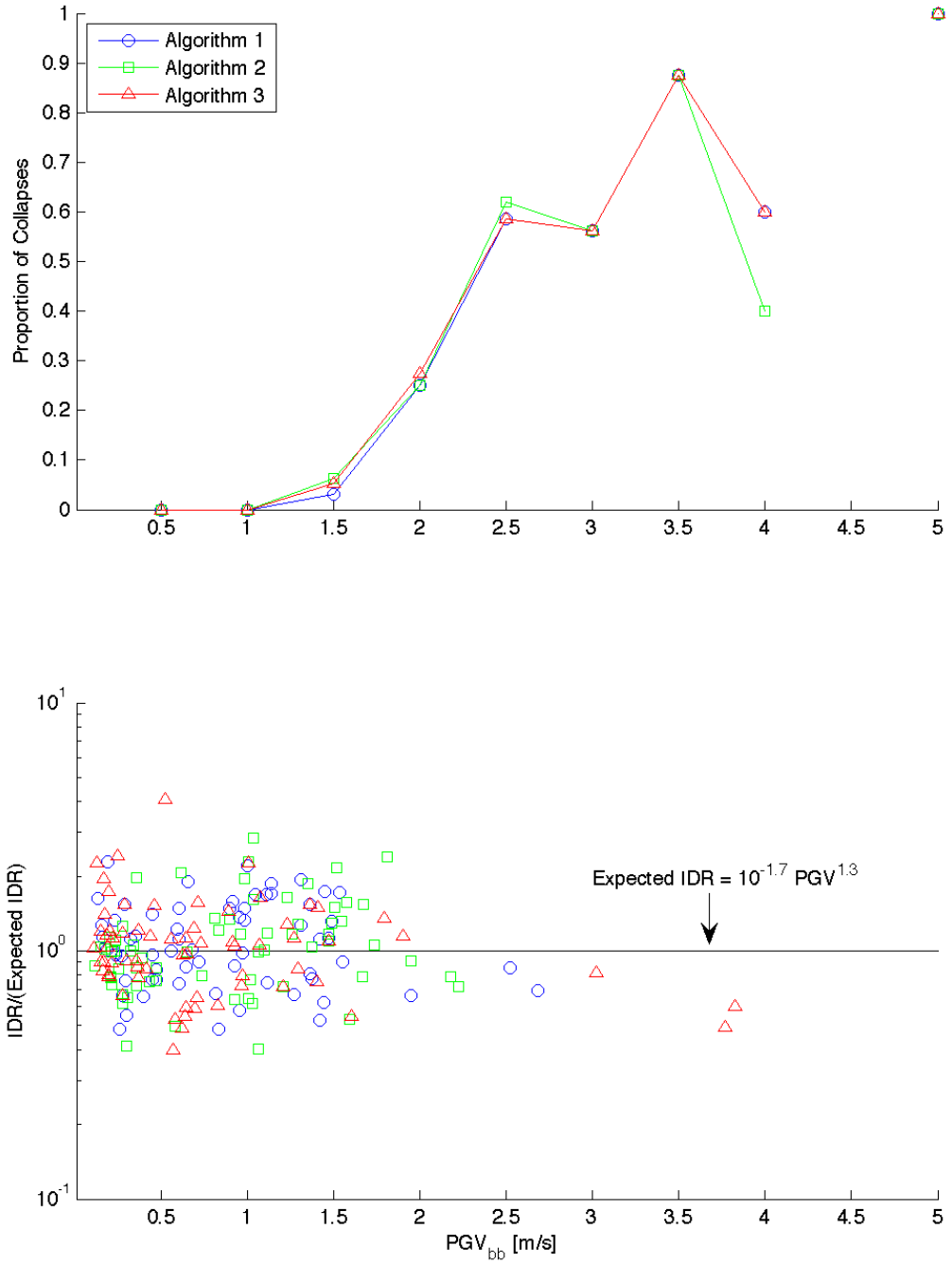

Figure 2.18: This figure compares the U20P model responses to ground motions with the resultant horizontal component determined by three algorithms. There is no systematic difference in the building response due to the algorithm that measures the peak-to-peak velocity.

2.7.2 Vertical Ground Motions

Seismic ground motions induce primarily lateral loads in buildings. In an earthquake the ground motions are three-dimensional, and thus an earthquake induces both lateral and vertical forces in buildings, along with moments. As a rule of thumb (codified in the building code), the vertical ground motion is approximately two-thirds of the horizontal motion. Also, buildings must withstand a constant downward acceleration of 1 g, which induces constant vertical loads. Thus buildings are inherently stronger vertically than laterally. For these reasons, engineers sometimes neglect vertical ground motions to simplify the model.

For the four building models, I simulate the building response with and without the vertical component of ground motion. Figure 2.19 maps the peak IDR. Based on this figure, there are no obvious differences in building response due to the presence of vertical ground motion. Figure 2.20 compares the building responses directly. The buildings collapse on similar proportions of sites with or without the vertical component. For $\mathrm{PGV_{bb}}$ at which there are differences, buildings subject to only the resultant horizontal component collapse on a slightly greater proportion of sites than do buildings subject to the vertical component as well. If both buildings at a site remain standing, the peak IDR is approximately the same if the vertical component is included or not. For large ground motions ($\mathrm{PGV_{bb}}$ greater than 2 m/s) neglecting the vertical component slightly over-predicts the probability of building collapse.

2.7.3 Brittle Weld Distribution

For models with brittle welds, each weld location has an assigned propensity to fracture. (Refer to Section 2.2.7 for a complete description of the weld model.) The finite element algorithm assigns each weld a fracture strain as a fraction of the yield strain ($\epsilon_{\mathrm{fracture}}/\epsilon_{\mathrm{yield}}$). If the strain in an individual weld fiber exceeds the fracture strain, the fiber does not carry tensile loads for the remainder of the simulation; it may carry compressive loads, though, if re-engaged. The random assignment of fracture strain to a weld samples from a user-specified distribution of fracture strains. Figure 2.8

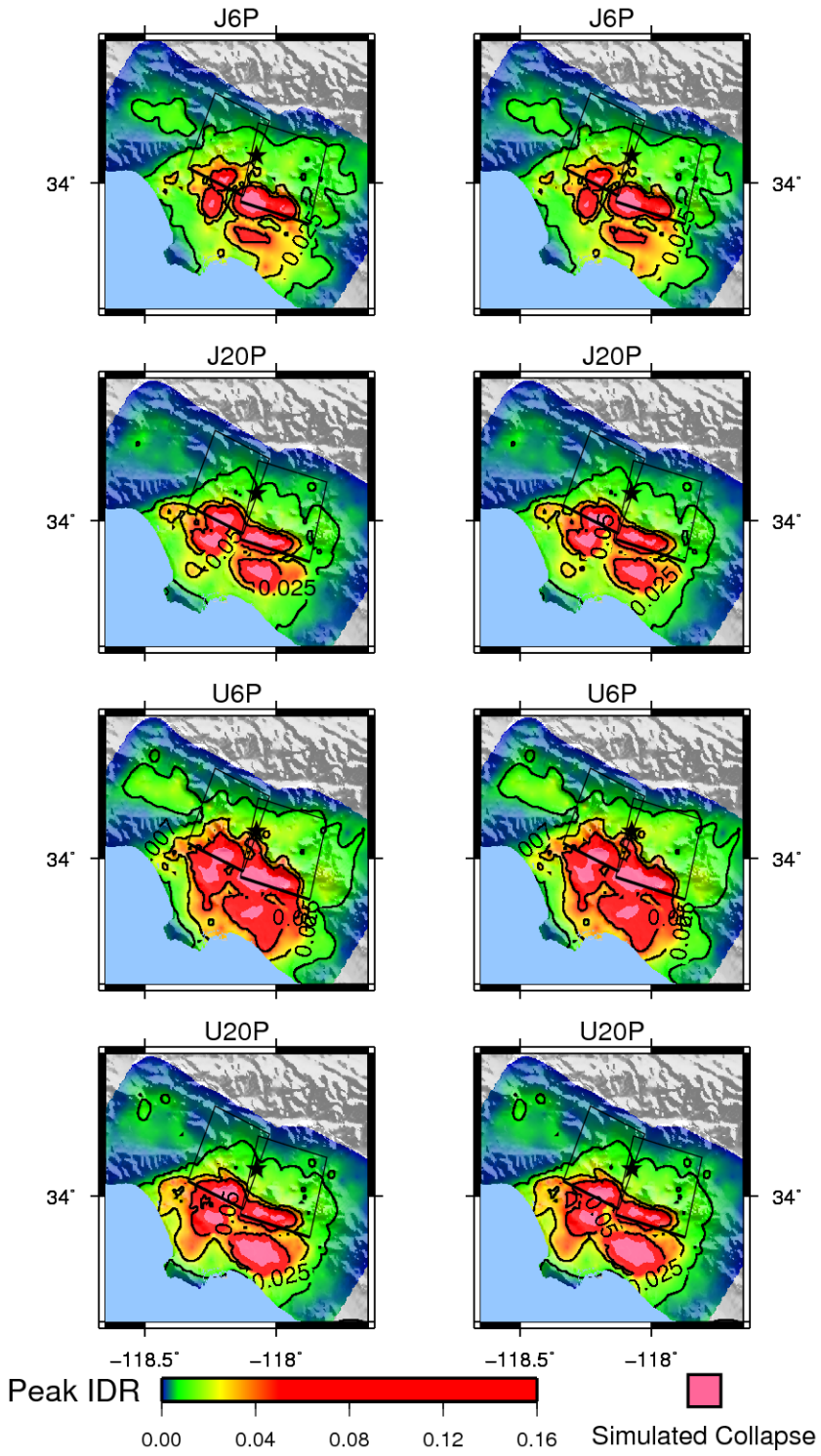

Figure 2.19: This figure compares building responses to ground motions with only the resultant horizontal component (maps on the left) and with both vertical and resultant horizontal components (maps on the right). There appears to be no difference in regional extent of building responses with or without the vertical component.

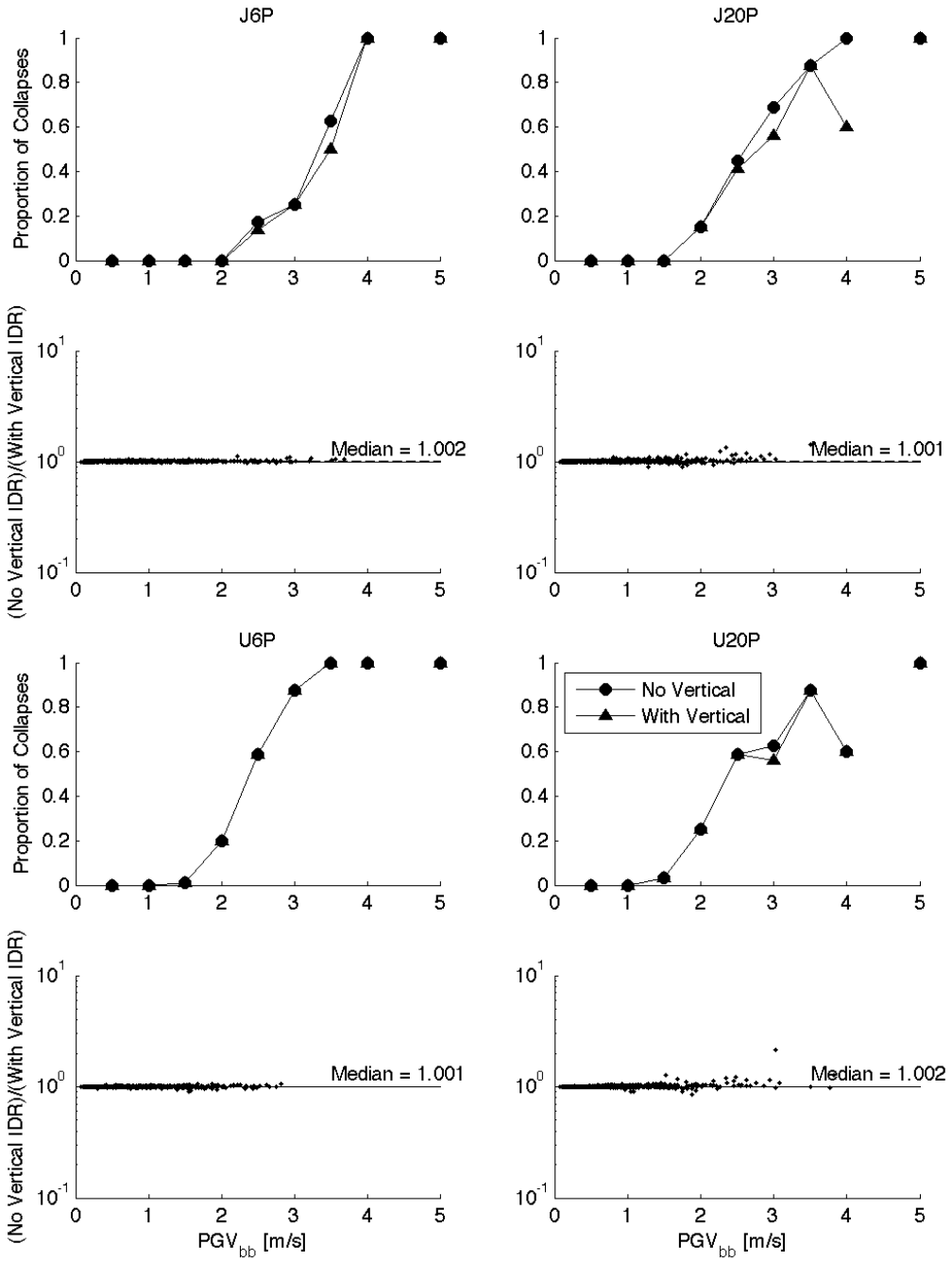

Figure 2.20: This figure compares the building responses to ground motions with and without the vertical component. For ground motions with a PGV_{bb} greater than 2 m/s, neglecting the vertical component may over-predict the number of collapses. However, this effect is insignificantly small.

shows two such weld fracture strain distributions.

I compare the simulated building responses for models with the B and F weld distributions. Figure 2.21 maps the peak IDRs for building models with each fracture strain distribution. The areal extent of large building responses (peak IDR greater than 0.025) is similar for the fracture strain models. Figure 2.22 directly compares the building responses at each site for the two fracture strain distributions. Models with F welds collapse on a consistently greater proportion of sites at a given PGV_{bb} than do models with B welds. If both models remain standing at a site, the peak IDR in the F weld building model tends to be larger than the peak IDR in the B weld model. For the smallest ground motions, there is no difference in peak IDR between the two models because no welds fracture. The weld model can cause different building responses only after the building yields and accumulates fractured welds. For larger ground motions, the peak IDR in F weld models is often 1.1–1.2 times larger then the peak IDR in B weld models and may be up to 4 times for some sites, depending on the building design.

There is no penultimate fracture strain distribution for this problem. The fracture strain distribution is necessary to model a random assignment of weld fracture strain to individual welds. The distribution can only be validated by experience, but there is little evidence from moment-resisting frames in ground motions as large as these. This thesis uses the B weld distribution in the following chapters. The choice of the F weld distribution would have resulted in larger building responses for building models with brittle welds.

2.7.4 Random Seed Number

The assignment of fracture strain to welds in the building model requires a seed number to generate the random sample of the fracture strain distribution. By chance, a seed number may cause an unusually large number of weak welds to be assigned to a localized area. In this case, the model may be inconsistent with an existing building, and certainly this is inconsistent with the purpose of randomly distributing the weld

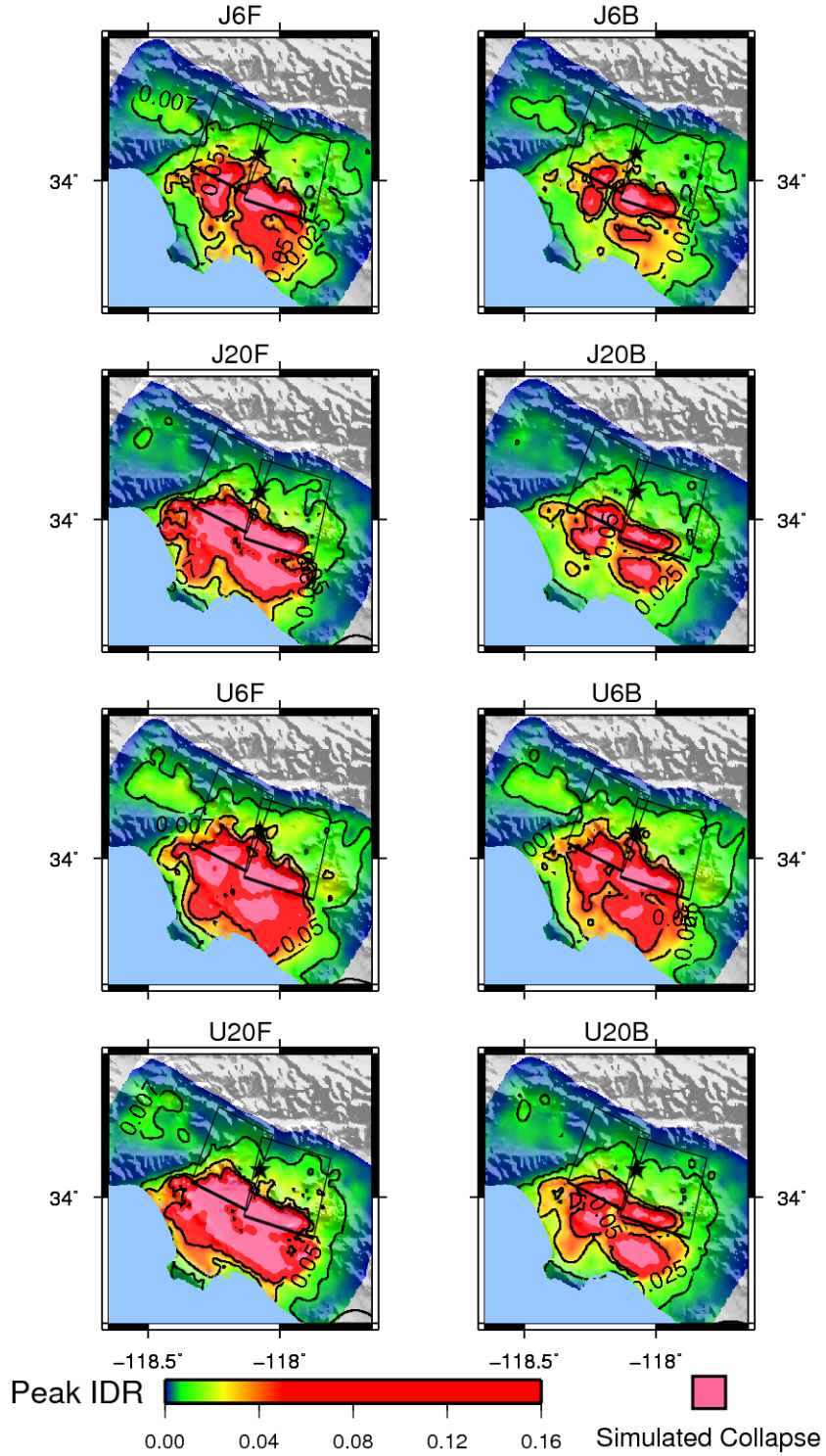

Figure 2.21: This figure compares building responses for models with brittle welds defined by the F weld (maps on left) and B weld (maps on right) distributions. There are differences in the responses at single sites, but the overall areal extent of large building response is consistent for the two weld fracture strain distributions.

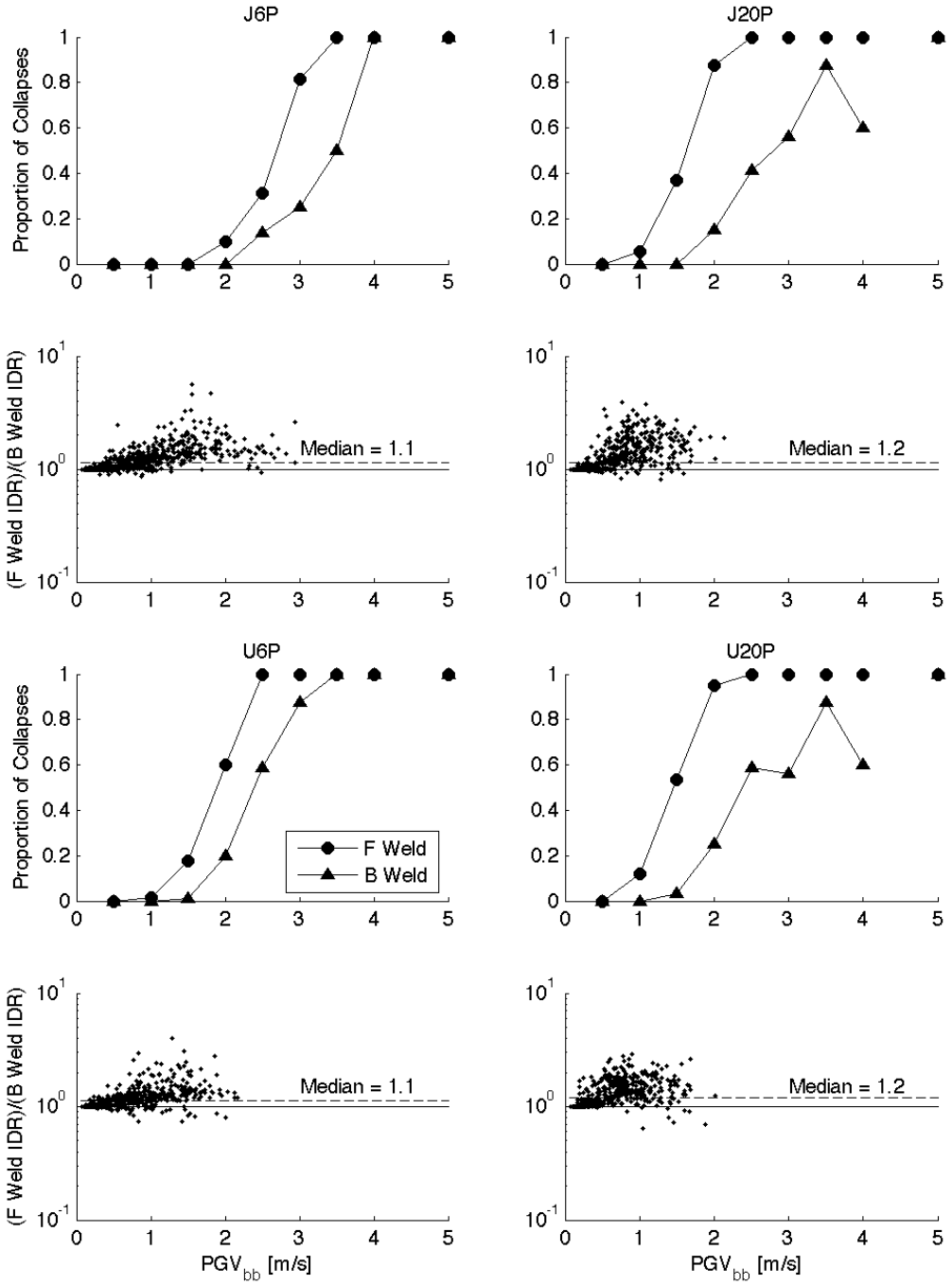

Figure 2.22: The assumed fracture strain distribution for brittle welds affects the building response. Models with F welds collapse on a greater proportion of sites than do models with B welds. If the models do not collapse, those with F welds have a peak IDR most likely 1.1–1.2 times the peak IDR for models with B welds.

fractures throughout the building. In this study, every brittle weld fracture strain assignment begins with the same seed number; models with the same weld fracture strain assignments sit at every site in the simulation domains.

To evaluate the effect of the random seed number on the building response, I compare the responses of four models, each with a different seed number. Figure 2.23 maps the peak IDRs for the twenty-story, more flexible building model with brittle welds (U20B). The areal extent of inelastic building response is similar for all four seeds, and the extent of the largest building responses (peak IDR greater than 0.05) is also similar. Figure 2.24 plots the building responses as functions of PGV_{bb}. There seems to be no consistent difference in building response due to the choice of seed number. The choice of one seed number over another does not contribute significantly to the uncertainty of the building response. The choice of weld fracture strain distribution (for example, B or F welds) affects the response of models with brittle welds more significantly than does the assignment of a sampled fracture strain to a particular weld.

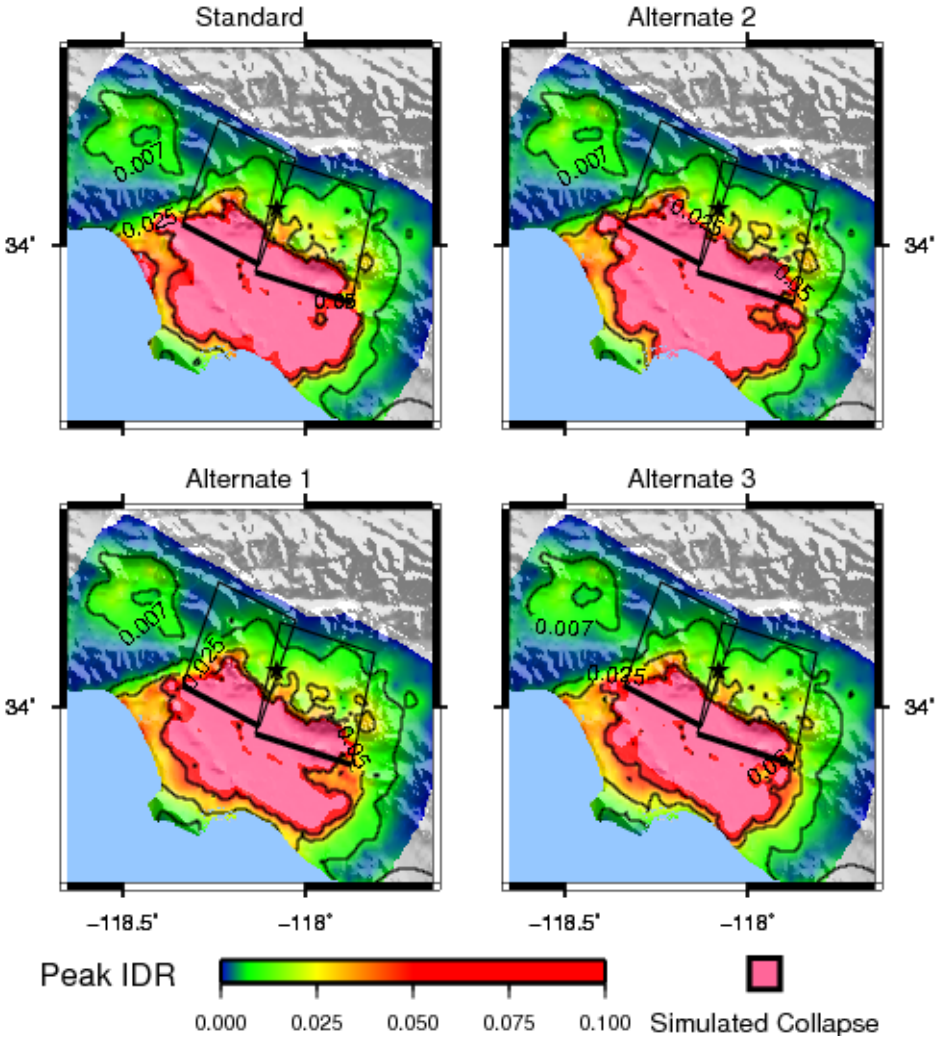

Figure 2.23: This figure compares the response of the U20B model with weld fractures assigned from four initial seed numbers. In each of the four simulations, the model at every site has the same weld fracture strain pattern within the building. While there are slight differences in the extent of building collapses, the models with welds assigned from different seed numbers appear to have similar responses at a given site.

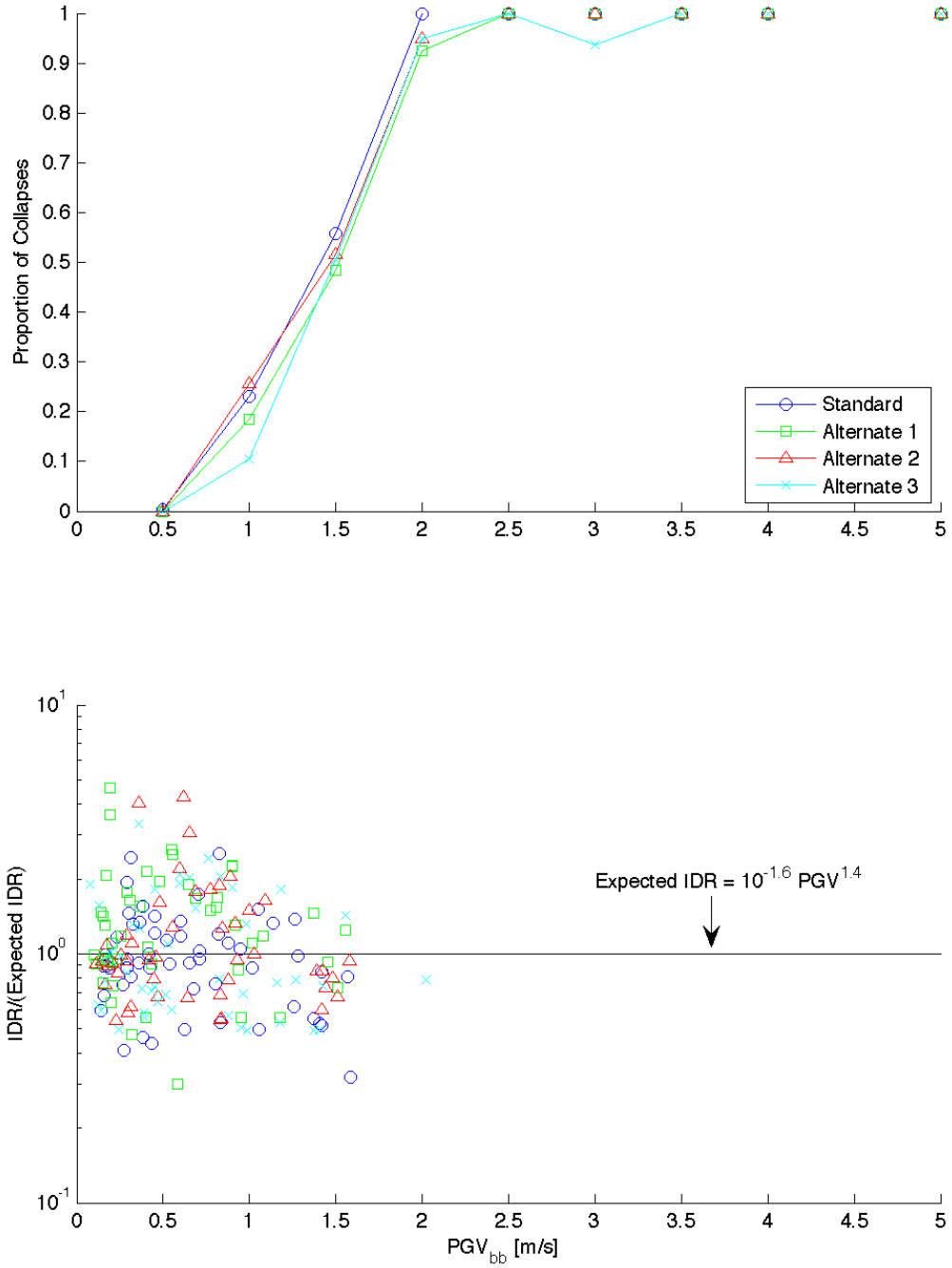

Figure 2.24: This figure compares the responses of brittle weld models with different assignments of fracture strains. Models with brittle weld fracture strains assigned from the four seed numbers considered here respond similarly to the same ground motions. This thesis uses the standard assignment for all brittle welds.